A COMPARISON OF TIME-OPTIMAL INTERCEPT TRAJECTORIES FOR THE F-8 AND F-15 - FINAL REPORT

January, 1990

Research Supported by
NASA Ames/Dryden Flight Research Facility
Grant No. NCC 2-506

Principal Investigator: Dr. Anthony J. Calise
Research Assistant: James B. Pettengill
NASA Grant Monitor: Eugene L. Duke

Georgia Institute of Technology
School of Aerospace Engineering
Atlanta, GA 30332

A COMPARISON OF TIME-OPTIMAL INTERCEPT TRAJECTORIES FOR THE F-8 AND F-15 - FINAL REPORT

SUMMARY

This report compares the simulation results of a real time control algorithm for onboard computation of time-optimal intercept trajectories for the F-8 and F-15 aircraft. Due to the inherent aerodynamic and propulsion differences in the aircraft, there are major differences in their optimal trajectories. The significant difference between the two aircraft are their flight envelopes. The F-8's optimal cruise velocity is thrust limited, while the F-15's optimal cruise velocity is at the intersection of the Mach and dynamic pressure constraint boundaries. This inherent difference necessitated the development of a proportional thrust controller for use as the F-15 approaches it's optimal cruise energy. Another interesting phenomena is that the optimal climb trajectory for the F-15 is along its dynamic pressure boundary. This necessitated the use of a sub-optimal proportional vertical lift controller to track the constraint boundary.

This report documents the application of singular perturbation theory to the trajectory optimization problem, along with a summary of the control algorithms. Numerical results for the two aircraft are compared to illustrate the performance of the minimum time algorithm, and to compute the resulting flight paths. A major recommendation is that future research be directed at the application of singular perturbation methods to problems in flight mechanics where state constraints, such as a maximum dynamic pressure limit, play an important role in the analysis.

This report documents a portion of the total research effort supported under this grant. The research related to time optimal aircraft pursuit evasion can be found in [4].

TABLE OF CONTENTS

	Page
SECTION 1- Introduction	1
SECTION 2 - Problem Formulation	2
SECTION 3 - Summary of Control Algorithm	4
3.1 Outer Solution	4
3.2 First Boundary Layer Solution	5
3.3 Second Boundary Layer Solution	6
3.4 Proportional Vertical Lift Control	7
3.5 Proportional Thrust Control	8
SECTION 4 - Numerical Results	10
SECTION 5 - Conclusions and Future Research	12
REFERENCES	13

LIST OF FIGURES

		Page
Figure 1.	Horizontal plane intercept geometry	14
Figure 2.	Flight envelope for the F-8 aircraft	15
Figure 3.	Flight envelope for the F-15 aircraft	15
Figure 4.	Ground tracks for cases 1-3	16
Figure 5.	Ground tracks for cases 1-3	16
Figure 6.	Commanded and actual altitude profiles for cases 1-3	17
Figure 7.	Commanded and actual altitude profiles for cases 1-3	17
Figure 8.	Altitude versus velocity for case 2	18
Figure 9.	Altitude versus velocity for case 2	18
Figure 10.	Comparison of full boundary layer optimization with sub-optimal proportional lift controller	19
Figure 11.	Desired and actual flight path angle profile for case 2	20
Figure 12.	Desired and actual flight path angle profile for case 2	20
Figure 13.	Lift and bank angle profile for case2	21
Figure 14.	Lift and bank angle profile for case2	21
Figure 15.	Thrust profile for case 2	22
Figure 16.	Thrust profile for case 2	22
Figure 17.	Ground track for case 4	23
Figure 18.	Ground track for case 4	23
Figure 19.	Commanded and actual altitude profiles for case 4	24
Figure 20.	Commanded and actual altitude profiles for case 4	24
Figure 21.	Altitude versus velocity for case 4	25
Figure 22.	Altitude versus velocity for case 4	25
Figure 23.	Lift and bank angle profile for case 4	26
Figure 24.	Lift and bank angle profile for case 4	26

SECTION 1
INTRODUCTION

There has been active research into optimizing flight path trajectories using multiple time scale separation techniques. In [1] Calise and Meorder showed that by using singular perturbation theory to separate the dynamics into fast and slow modes and then applying the optimality conditions from calculus of variations, one could obtain a closed form solution to the min-time intercept problem. What soon followed was a 3-D real-time piloted simulation and which used aerodynamic and propulsion data from the F-8 [2]. The algorithm was eventually flight tested on the NASA F-8 test aircraft at NASA Ames/Dryden Flight Research Facility [3]. The objective of this research was to modify the existing algorithm for use on an F-15 aircraft.

This report documents the results of modifying the min-time intercept algorithm from the F-8 to F-15, which represents a portion of the activity supported under this research grant. A portion of this work was conducted at NASA Ames/Dryden Flight Research Facility during the summer 1989. This report will contain four sections. The problem formulation is given in Section 2. A summary of the control algorithm is given in Section 3, which highlights the application of singular perturbation theory along with the optimality conditions derived from calculus of variations. This development could have been explained in full detail, however, in the interest of brevity only the first two boundary layer approximations will be discussed. This also coincides with the fact that a sub-optimal proportion lift controller was used on the F-15 due to the fact that the optimal trajectory rides the dynamic pressure constraint. Section 4 presents numerical results comparing the F-8 and F-15. Section 5 gives the conclusions for this work and identifies future work which needs to be accomplished prior to a flight test.

SECTION 2
PROBLEM FORMULATION

The point mass equations of motion are referenced to a horizontal, target centered, inertial coordinate frame illustrated in Fig. 1

$$\dot{x} = V\cos\gamma\cos\beta \tag{1}$$
$$\dot{y} = V\cos\gamma\sin\beta - V_T\cos\gamma_T \tag{2}$$
$$\varepsilon\dot{E} = (T-D)V/W \tag{3}$$
$$\varepsilon^2\dot{\beta} = L\sin\mu/mV\cos\gamma \tag{4}$$
$$\varepsilon^3\dot{h} = V\sin\gamma \tag{5}$$
$$\varepsilon^4\dot{\gamma} = (L\cos\mu - W\cos\gamma)/mV \tag{6}$$

These equations are valid for constant weight, thrust aligned with the flight path, and flat earth approximations. $E \equiv h + V^2/2g$ is the total aircraft energy per unit weight, β is the heading angle, h the altitude, γ the flight path angle, and μ the bank angle. Drag is assumed to have conventional parabolic form

$$D = qSC_{D_0} + KL^2/qS, \qquad q = \rho V^2/2 \tag{7}$$

where q is the dynamic pressure, ρ the air density and

$$K = \eta / CL_\alpha \tag{8}$$

Lift is defined by

$$L = qSCL_\alpha\alpha \tag{9}$$

where α is the angle of attack. The control variables are L, μ, and thrust T. The objective is to find the controls L, μ, T that minimize the time to intercept a constant velocity target

$$J = \int_0^{t_f} dt \tag{10}$$

The minimization is subject to the following state and control variable constraints:

$$L \leq W\, G_{max} \tag{11}$$

$$L \leq qS\, C_{L_\alpha} \alpha_{max} \tag{12}$$

$$T_{min}(h,V) \leq T_{max}(h,V) \tag{13}$$

$$q \leq q_{max},\ V \leq V_{max} \tag{14}$$

where G_{max} is the maximum load factor, α_{max} the maximum angle of attack, T_{min} and T_{max} the thrust level limits that are functions of aircraft altitude and velocity. The boundary conditions are such that the initial aircraft state is fully specified and require

$$x(t_f) = y(t_f) = 0,\ h(t_f) = h_T(t_f) \tag{15}$$

for intercept, where $h_T(t_f)$ is taken as the projected target motion in altitude

$$h_T(t_f) = h_T(0) + (V_T \sin\gamma_T) t_f \tag{16}$$

The parameter ε designates multiple time scaling used to order the dynamics [1]. The approach here is to find a solution for $\varepsilon = 1$ by an power series expansion around $\varepsilon = 0$. The boundary layers are separated by rescaling time as $\tau_i = t / \varepsilon^i$, $i = 1,...,4$, respectively, then setting $\varepsilon = 0$ in the resulting equations. A justification for this specific ordering of the dynamic equations is given in [1].

SECTION 3
SUMMARY OF CONTROL ALGORITHM

3.1 Outer Solution

In the outer solution, the controlled aircraft is assumed to be traveling on a fixed course at a constant speed, as can be seen by letting $\varepsilon \rightarrow 0$ in Eqs. (3-6). This addresses only the x and y dynamics, and the states β, h, and E take on the role of control like variables. In order to satisfy the intercept requirements, we have the following constraint

$$V \sin(\beta - \lambda) = V_T \cos\gamma_T \cos\lambda \tag{17}$$

This means that there is no relative motion allowed perpendicular to the horizontal line-of-sight axis. The optimal controls h_0 and E_0 are determined from minimizing the reduced Hamiltonian

$$H_0(E,h_1) = \lambda_{x0} V\cos\beta + \lambda_{y0}(V\sin\beta - V_T\cos\gamma_T) + 1 = 0 \tag{18}$$

and it is shown in [1] that this reduces to

$$h_0, E_0 = \arg\max_{h,E}(V) \tag{19}$$

where the maximization takes place subject to the constraints in Eqs. (11-14) and subject to the following conditions that result from setting $\varepsilon=0$ in (3-6)

$$T = D_0, \quad \mu_0 = 0, \quad \gamma_0 = 0, \quad L_0 = W \tag{20}$$

The term D_0 in (20) is drag for L = W

$$D_0 = q_0 S C_{D_0} + KW^2 / q_0 S \tag{21}$$

where

$$q_0 = \rho(h_0)V_0^2/2, \quad V_0 = \sqrt{2g(E_0 - h_0)} \tag{22}$$

The subscript 0 denotes the zeroth or outer solution. The maximization in (19) is equivalent to finding the maximum velocity cruise point.

The cruise point solution from Eq. (19) for the F-8 and F-15 aircraft are displayed in Figs. 2 and 3, superimposed upon their flight envelopes. Note that since the F-8 is thrust limited, its

cruise point lies on the T_{max}=D contour. The F-15 is q and Mach limited, and its cruise point lies at the intersection of these constraint boundaries. Thus T does not equal T_{max} in the outer solution for the F-15.

The optimal cruise heading β_0 is computed using (17)

$$\beta_0 = \sin^{-1} (V_T \cos \gamma_T \cos \lambda / V_0) + \lambda \tag{23}$$

The costates λ_{x0} and λ_{y0}, associated with the horizontal position dynamics in the outer control solution are needed in subsequent boundary layer solutions. These take the form

$$\lambda_{x0} = -\cos \beta_0 / (V_0 - V_T \cos \gamma_T \cos \beta_0) \tag{24}$$
$$\lambda_{y0} = -\sin \beta_0 / (V_0 - V_T \cos \gamma_T \cos \beta_0) \tag{25}$$

These are determined from the optimality conditions $\partial H_0 / \partial \beta = 0$ and the condition $H_0 = 0$. It should be noted that the cruise solution for h_0 and E_0 is independent of target motion and intercept geometry. This allows these quantities to be calculated off line and stored. The only outer solution calculations performed on-line are Eqs. (23), (24), and (25).

3.2 First Boundary Layer Solution

The first boundary layer addresses only the energy dynamics. The constraints

$$\mu_1 = 0, \quad \gamma_1 = 0, \quad L_1 = W \tag{26}$$

arise from Eqs. (4-6) when the time transformation $\tau = t / \varepsilon$ is introduced and we let $\varepsilon \rightarrow 0$. The control like variables are T, h and β. The optimal β is the same as in the outer solution. Since T appears linearly in the Hamiltonian,

$$T_1 = T_{max} (h,V), \text{ when } \lambda E_1 < 0 \tag{27}$$
$$T_1 = T_{min} (h,V), \text{ when } \lambda E_1 > 0 \tag{28}$$

This corresponds roughly to an energy climb and energy descent, respectively. Optimization with respect to h yields for climb

$$h_f^c = \arg \max_h \left\{ \frac{(Tmax - Do)V}{V - Vo} \right\}_{E = Ecurrent} \quad Tmax \geq D_o \tag{29}$$

and descent

$$h_f^d = \arg \min_h \left\{ \frac{(Tmin - Do)V}{V - Vo} \right\}_{E = Ecurrent} \quad Tmax \leq D_o \tag{30}$$

The climb path to cruise for the F-8 and F-15 are superimposed on the aircraft flight envelopes in Figs. 2 and 3. The optimal descent path for both aircraft is along the q_{max} boundary. The expression for the first boundary layer costate is

$$\lambda E_1 = -WH_0 (E, h_1) / V_1 (T_1 - D_0) \tag{31}$$

where H_0 is the outer solution Hamiltonian evaluated at the first boundary layer conditions. Since the solutions for h_1^c and h_1^d are independent of target motion, they can be precomputed and stored as a function of E. Only the energy costate variable in (31) is computed on-line.

3.3 Second Boundary Layer Solution

The second Boundary layer solution determines the optimal heading angle dynamics. Introducing the time stretching transformation $\tau = t / \varepsilon^2$ and letting $\varepsilon \rightarrow 0$ while holding the slow dynamics x, y and E fixed, yields the constraints

$$\gamma_2 = 0, \quad L^2 = L^2_{22} + W^2 \tag{32}$$

where L is the total lift and $L_{22} = L \sin \mu$, the horizontal component of lift. The control variables are T, h and L_{22}. Assuming that all turning takes place near the initial time where $\lambda E_1 < 0$, the optimal thrust is

$$T_2 = T_{max} (h_2, V_2) \tag{33}$$

where h_2 is the optimal commanded altitude determined by

$$h_2 = \arg \min_h \{-\rho / KV H_1 (E, h, \beta)\}|_{E=Ecurrent,\ \beta=\beta current} \tag{34}$$

In Eq. (34) $H_1(E, h, \beta)$ is the Hamiltonian in the first boundary layer evaluated at the current

values of E, h and β. It is expressed as

$$H_1(E, h, \beta) = \lambda_{x0} V\cos\beta + \lambda_{y0} (V\sin\beta - V_T \cos\gamma_T) + \lambda_{E1} [(T - D_0)V / W] + 1 = 0 \qquad (35)$$

The solution for the horizontal lift component L_{22} is

$$L_{22} = \sqrt{-qSWH_1(E,H,\beta)/(VK\lambda_1^E)} * \text{sign}(\beta_o - \beta) \qquad (36)$$

3.4 Proportional Vertical Lift Control

An option was included in the algorithm for stopping the singular perturbation analysis after the second boundary layer, and employing a sub-optimal vertical lift solution. It was necessary in this study to use this option due to the fact that zero order singular perturbation analysis results in a steady state error when following ramp like altitude commands. Although this steady error is not a critical factor for the F-8 study in [1], it is essential to accurately track the altitude command for the F-15 since the optimal climb path lies essentially along the dynamic pressure constraint (Fig. 3). The derivation of the control logic proceeds as follows. From Eq. (5)

$$\dot{h} = V\sin\gamma \qquad (37)$$

We would like the altitude rate to track the altitude error according to proportional feedback control

$$\tau_h \dot{h} = h_2 - h. \qquad (38)$$

where τ_h is the time constant associated with the decay in altitude error. Since h_2 is not a constant command signal, but more like a ramp command, a term must be included to account for the steady state error that would otherwise result. The rate of change in h_2 can be estimated using

$$\dot{h}_2 \approx \dot{h}_1 = \frac{\partial h_1}{\partial E}\dot{E} = V_1 \sin\gamma_1 \qquad (39)$$

where $\partial h_1/\partial E$ is the slope associated with altitude with respect to E along the dynamic pressure boundary (Fig. 3). In (39) we have used the fact that $h_2(E) = h_1(E)$ when the heading error is near zero. The desired flight path angle γ_d is formed by summing γ from (37) and (38) with γ_1, from (39). Using small angle approximation for $\sin\gamma$ we have

$$\gamma_d = \frac{\dot{E}\,\partial h}{V_1 \partial E} + \frac{(h_2\text{-}h)}{\tau_h V} \tag{40}$$

With γ_d defined we can calculate the vertical lift component. Using Eq. (6)

$$\dot{\gamma} = (L_1 - W\cos\gamma) / mV = \tau_\gamma (\gamma_d - \gamma) \tag{41}$$

where τ_γ is the time constant associated with the decay in flight path angle error. As an alternative, τ_γ and τ_h can be related to a desired natural frequency and damping ratio [1]. Solving for L_1 yields

$$L_1 = mV\tau_\gamma (\gamma_d - \gamma) + W\cos\gamma \tag{42}$$

The relationship between the vertical and horizontal lift components along with the bank angle are given by

$$\mu = \arctan\frac{L_2}{L_1} \qquad L = \sqrt{L_1^2 + L_2^2} \tag{43}$$

where L_2 is the horizontal component of lift.

3.5 Proportional Cruise Thrust Control

Since the flight envelope for the F-8 has as its V_{max} cruise point at a T=D point the throttle setting was set at full throttle. This means that the F-8 will asymptotically reach its optimal cruise energy. In other words it never theoretically attains the desired optimal cruise energy. The F-15 flight envelope has as its V_{max} cruise point at the intersection of the q_{max} limit and M_{max} limit. With the cruise point at this location the F-15 reaches its optimal cruise energy in finite time. By virtue of its high T/W ratio the F-15 can gain energy at a much higher rate compared to that of the F-8. Therefore in the case of the F-15 it is necessary to throttle back as the cruise energy is approached. This throttling was incorporated into the algorithm by use of a proportional controller, the derivation of which is described as follows. Since it is desired that the energy rate track the error in energy, which is constant during cruise, we have from Eq. (3)

$$\dot{E} = (T\text{-}D)\,V / W = (E_c\text{-}E)/\tau_E \tag{44}$$

Solving for T gives

$$T = W (E_c - E) / \tau_E V + D \tag{45}$$

where τ_E is the controller time constant set to give the desired rate of decay in the energy error.

The procedure for throttle control during descent was the same as that used in the F-8 study described in [1]

SECTION 4
NUMERICAL RESULTS

Figures 4 and 5 show the ground tracks for Cases 1-3. Both simulations have the same initial geometry. The target flies at a constant altitude, velocity and heading but with differing downrange initial distances. These differing initial distances demonstrate the algorithms range-matching calculation of an optimal pseudo-cruise point [1]. Notice the rapid closure rate of the F-15 as compared to the F-8. Figures 6 and 7 show the altitude and optimal commanded altitude (h_2) time histories. The time constants τ_h and τ_γ were set to correspond to a damping ratio and natural frequency of 1.0 and 0.1 respectively. Case 1 is a long range intercept which is comprised of three phases; an initial climb along the optimal climb path followed by a cruise leg at the aircraft's optimal cruise energy (E*, h*), then a descent portion along the dynamic pressure boundary to intercept the target. Cases 2-3 being shorter intercepts never obtain their optimal cruise energies due to their proximity to their targets. These cases obtain pseudo-cruise energies instead [1]. In these cases the aircraft climbs to a pseudo-cruise energy and immediately initiates descent. Notice in each of the F-8 simulations the optimal commanded altitude has peaks between 150 and 175 seconds for each case. These demonstrate the characteristic dive in the transonic region. In contrast, the F-15 has enough thrust to simply ride the dynamic pressure boundary. Another interesting feature can be seen in comparing the Case 2 time histories. The F-8 never reaches its optimal cruise energy. Instead it approaches a lower pseudo-cruise energy. The F-15 has sufficient energy rate capacity to reach its optimal cruise energy at this shorter intercept range. The Case 2 optimal climb paths are compared in Figs. 8 and 9. In the F-8 simulation notice the near constant velocity energy climb followed by the characteristic transonic dive. The F-15 climb profile is along the dynamic pressure boundary. There exists a slight dynamic pressure boundary violation in the figure, however, this can be improved by tuning the gains τ_h, τ_γ and τ_E

Figure 10 is a comparison of optimizing the h and γ dynamics [1] versus using the sub-optimal proportional lift controller. Notice the underdamped response of the optimized boundary layers results in severe dynamic pressure constraint boundary violations. This is due to separating the h and γ dynamics into separate boundary layers which has to be done in order to obtain a closed form solution. The suboptimal proportional lift controller allows the designer to pick the gains so as to avoid a q_{max} violation. Figures 11 and 12 show the flight path angle and desired flight path angle time histories. In both simulations, descent initiation is clearly evident by the sudden decrease in the desired flight path angle. Also notice that the flight path angle never exceeds 0.2 rad during climb, which validates the $\gamma = 0$ approximation in the first and second boundary layer

analysis. It can also be seen that the F-15 completes the intercept in nearly half the time it takes the F-8. The lift and bank angle profiles are shown in Figs. 13 and 14. Note that both aircraft bank 180 degrees in order to initiate descent. In the F-15 simulation, the sudden decrease in lift at 115 seconds is due to the approaching optimal cruise velocity, where the throttle control in (45) is initiated. This changes the energy rate term in (40), and consequently the vertical lift calculated in (42). In Figs. 15 and 16 the thrust histories for each aircraft are given. The time constant τ_E here was set to 6 seconds. Descent initiation is evident by the sharp decrease in thrust at 150 and 350 seconds for the F-15 and F-8 respectively. In the F-15 simulation, at 115 seconds the proportional thrust controller throttles back the engines just prior to the aircraft obtaining its pseudo-cruise energy level.

The ground tracks for Case 4 are given in Figs. 17 and 18. This case is a close in intercept which has the target moving at constant altitude, velocity and heading 180 degrees in the opposite direction. This case illustrates a combined initial hard turn and climb (yo-yo maneuver) followed by a descent under near tail chase conditions. The pursuer's initial altitude is identical to that of the target and the velocity is above the corner velocity for that altitude. Note that the downrange intercept distance is considerably less for the F-15 aircraft. Figures 19 and 20 give the altitude and commanded altitude time histories. Both aircraft perform a high speed yo-yo maneuver in order to trade speed for increased turning performance. It is interesting to note that the time to complete the hard turn is nearly identical for both aircraft, 10 seconds. The reason for the large altitude command is due to the large initial heading errors. The jump in commanded altitude is at the completion of the hard turn so as to get on the optimal climb path. Between 10 and 20 seconds the F-8 dives to trade potential energy for kinetic energy, while the F-15 just accelerates to intercept. Figures 21 and 22 show altitude versus velocity plots for Case 4 where the high speed yo-yo maneuvers are more evident. Both simulations show the aircraft moving initially toward the corner velocity to trade speed for increased turning performance. Once the turn is completed both aircraft move to get on the optimal climb path which is followed by a descent along the dynamic pressure boundary. Figures 23 and 24 show the lift and bank angle profiles. Both aircraft initiate maximum G turns at 0-10 seconds to reduce the heading error. This is followed by a climb phase followed by cruise then descent at 40 and 90 seconds for the F-15 and F-8 respectively. In the F-15 simulation it is evident that throttling is taking place at 28 seconds due to the decrease in lift. Also note the large lift at interception, this indicates that the F-15 is tending to miss the target. This is due to the higher degree of coupling in the dynamics for the F-15, which requires further investigation.

SECTION 5
CONCLUSIONS AND FUTURE RESEARCH

The differences in the numerical results between the F-8 and F-15 trajectories lie mainly in each aircraft's ability to gain energy. The F-8 is an aircraft which never encounters any state constraint boundaries during its climb phase. The F-15's higher thrust to weight ratio allows the aircraft to gain energy at a much higher rate. Since the F-15's flight trajectory lies on the dynamic pressure boundary, the methodology for optimizing the altitude and flight path angle dynamics in [1] does not apply. This was circumvented by the application of the sub-optimal proportional lift and thrust controllers which provided an adequate sub-optimal solution. It was noticed that setting the time constants τ_h, τ_γ and τ_E to achieve the best performance for long range intercepts gave poor close-in intercept performance. This problem would imply that these gains are maneuver dependent, which it not satisfactory for real time implementation. A solution to this problem is to attempt to optimize the altitude and flight path angle dynamics, subject to the dynamic pressure constraint.

The major recommendation for future research is that the singular perturbation methodology in [1] be extended to address the issue of state constrained optimization problems. This would avoid the gain scheduling issue described above. Another interesting point worth investigating is the assumption of thrust aligned along the velocity vector. Thrust is actually aligned with the body axis. This reduces the thrust component due to the angle of attack dependence that would appear in the energy rate equation.

REFERENCES

1. Calise, A. J., and Moerder, DD. D., " Singular Perturbation Techniques for Real-Time Aircraft Trajectory Optimization and Control," NASA CR-3597, August 1982.

2. Calise, A. J., Moerder, DD. D., and Price, D. B., " Piloted Simulation of an Onboard Trajectory Optimization Algorithm," *Journal of Guidance and Control*, Vol. 7, No. 3, May-June 1984, pp. 355-360.

3. Jones, F. P., Duke, E. L., and Calise, A. J., "Flight Test Experience from a Three-Dimensional Optimal Intercept of a Maneuvering Target," 2nd International Symposium on Differential Games, Williamsburg, VA, August 1986.

4. Menon, P. K., and Duke, E. L., " Time Optimal Aircraft Pursuit-Evasion with a Weapon Envelope Constraint-Final Report," Georgia Institute of Technology, January 1990.

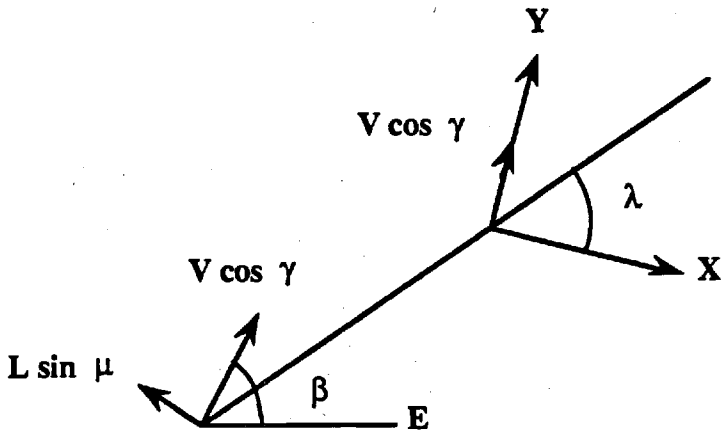

Figure 1. Horizontal plane intercept geometry

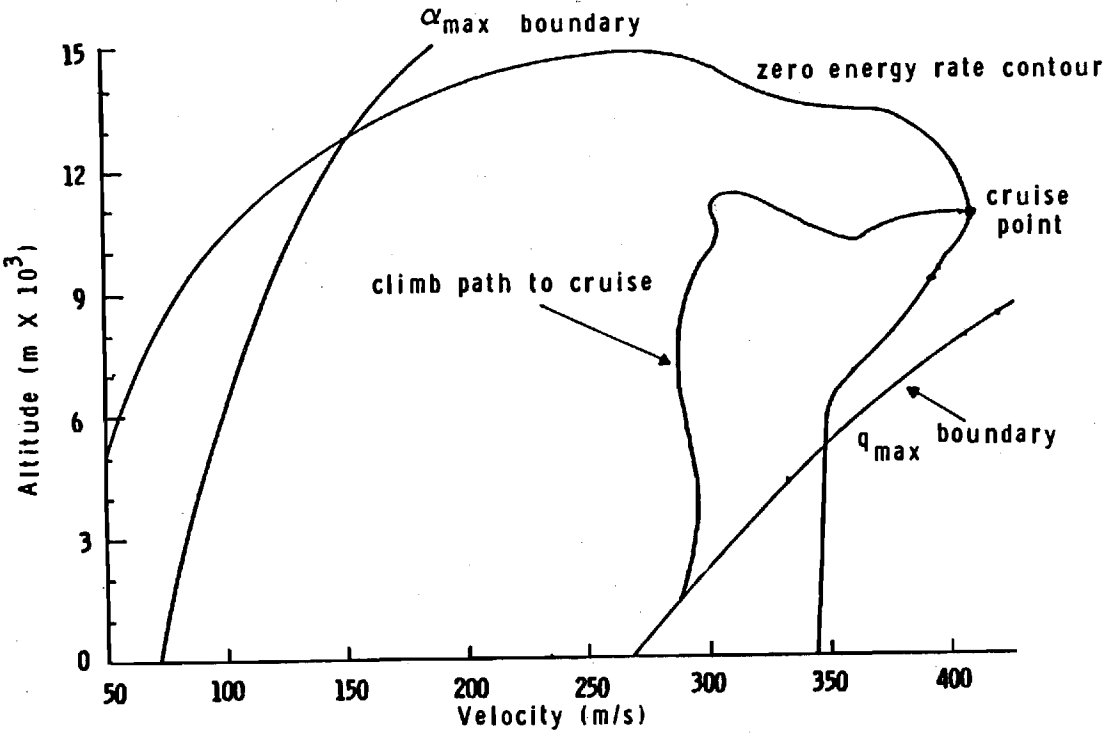

Figure 2. Flight envelope for the F-8 aircraft

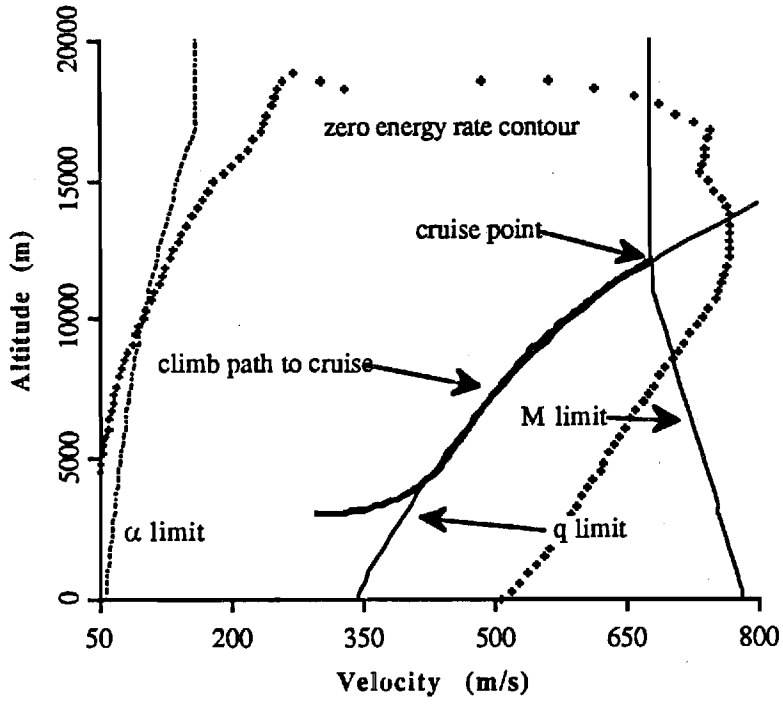

Figure 3. Flight envelope for the F-15 aircraft

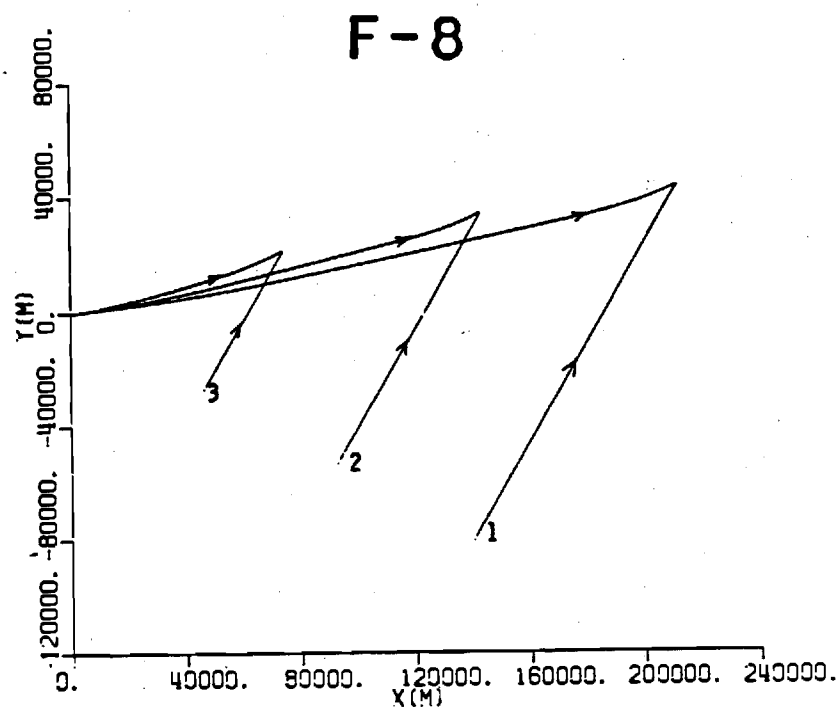

Figure 4. Ground tracks for cases 1-3

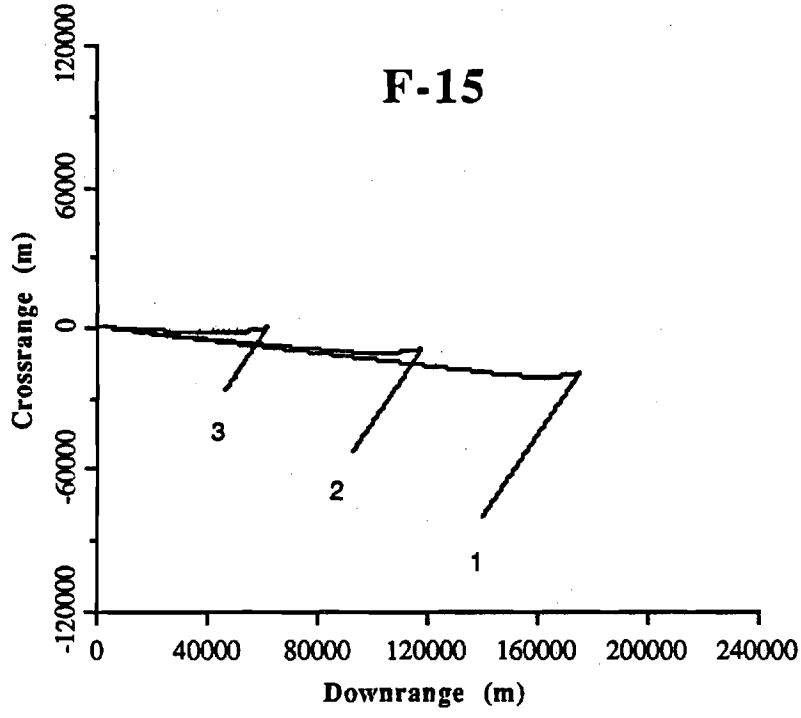

Figure 5. Ground tracks for cases 1-3

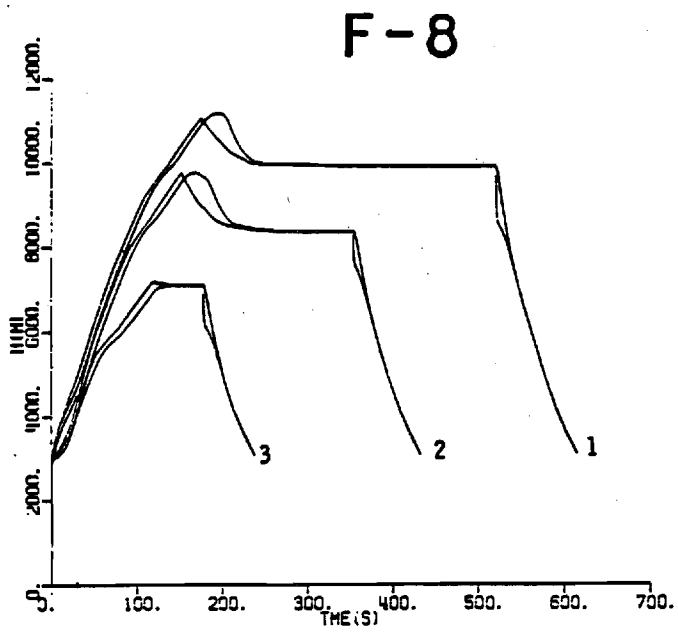

Figure 6. Commanded and actual altitude profiles for cases 1-3

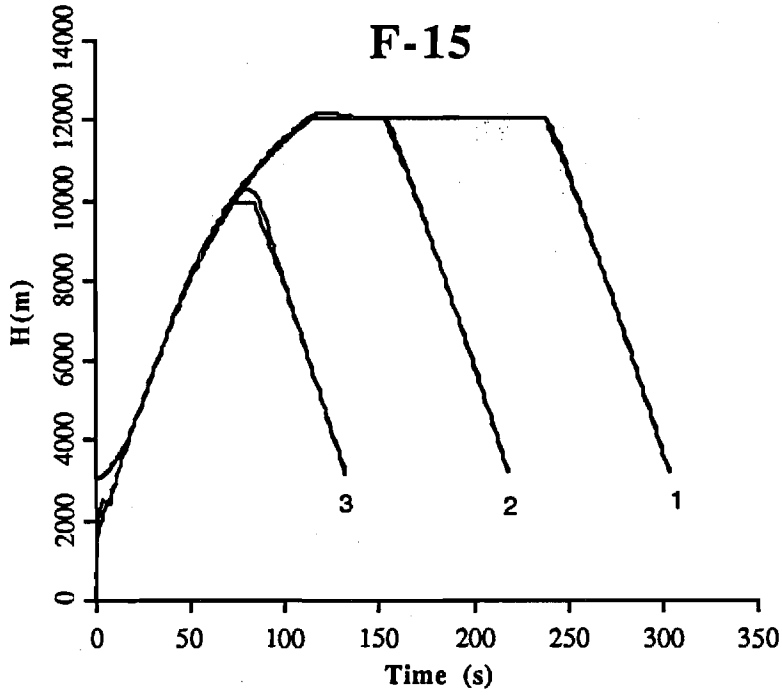

Figure 7. Commanded and actual altitude profiles for cases 1-3

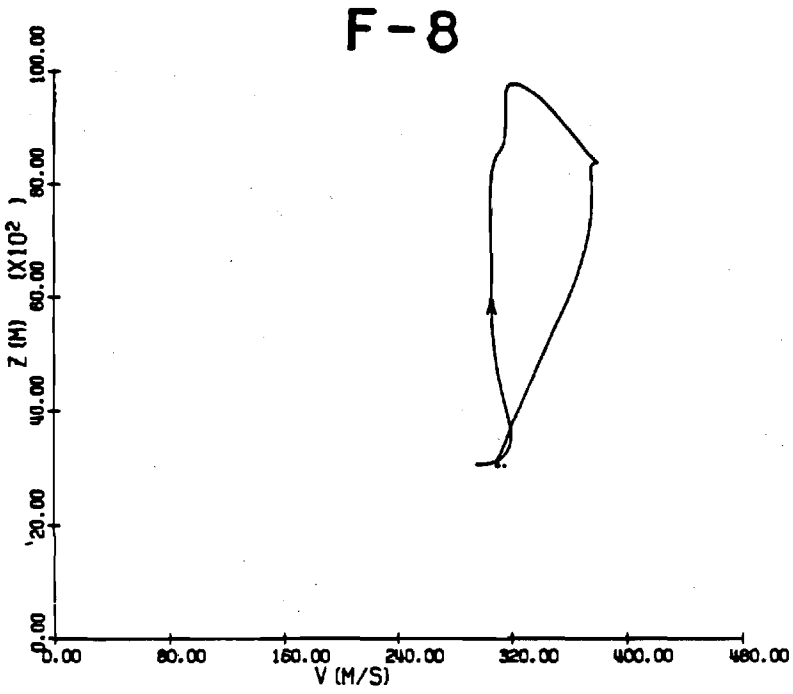

Figure 8. Altitude versus velocity for case 2

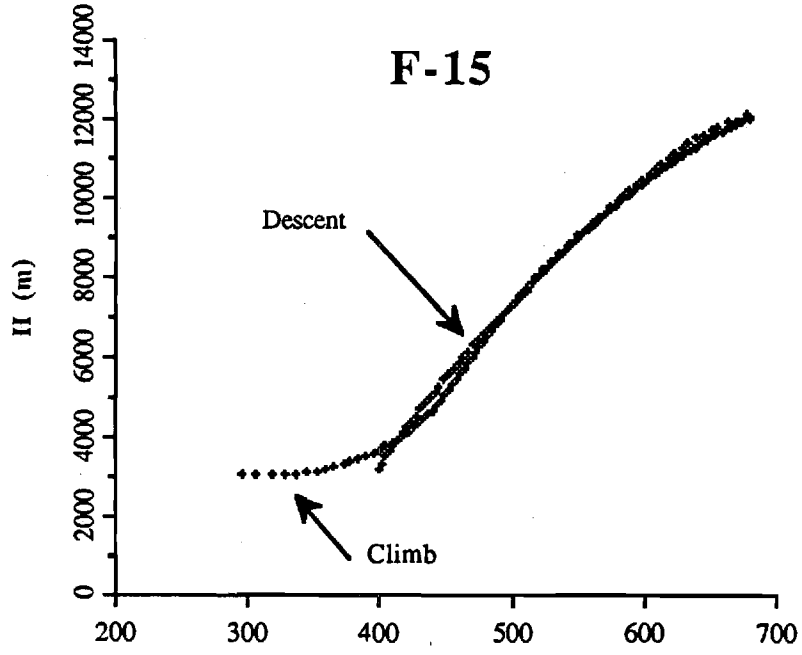

Figure 9. Altitude versus velocity for case 2

Comparison of Numerical Results:

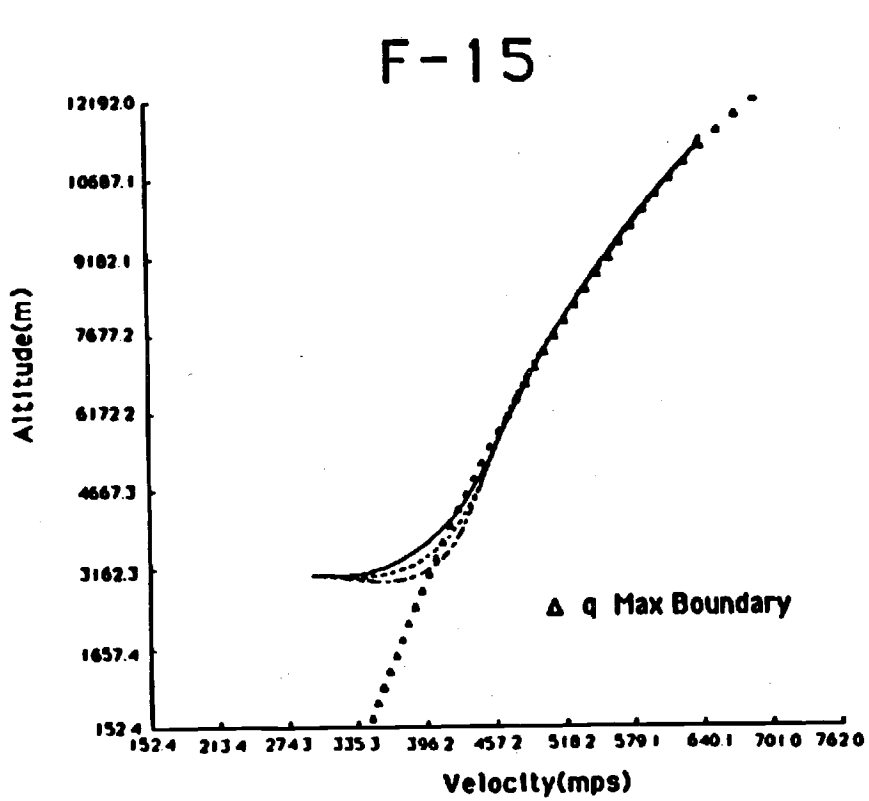

Altitude vs Velocity for 3 values of Ωn and ζ

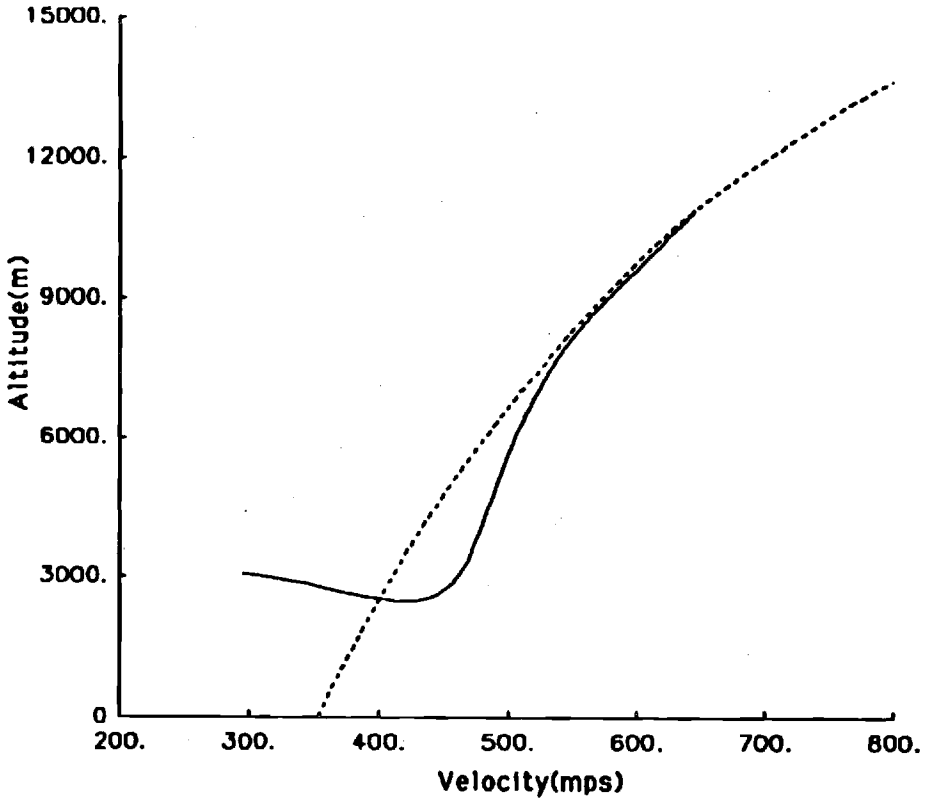

Altitude vs Velocity for 3rd and 4th Boundary Layer Optimization

——— ζ = 1.00 t_s = 22.5 sec
-------- ζ = 0.85 t_s = 22.5 sec
—·—·— ζ = 0.70 t_s = 22.5 sec

Figure 10. Comparison of full boundary layer optimization with sub-optimal proportional lift controller

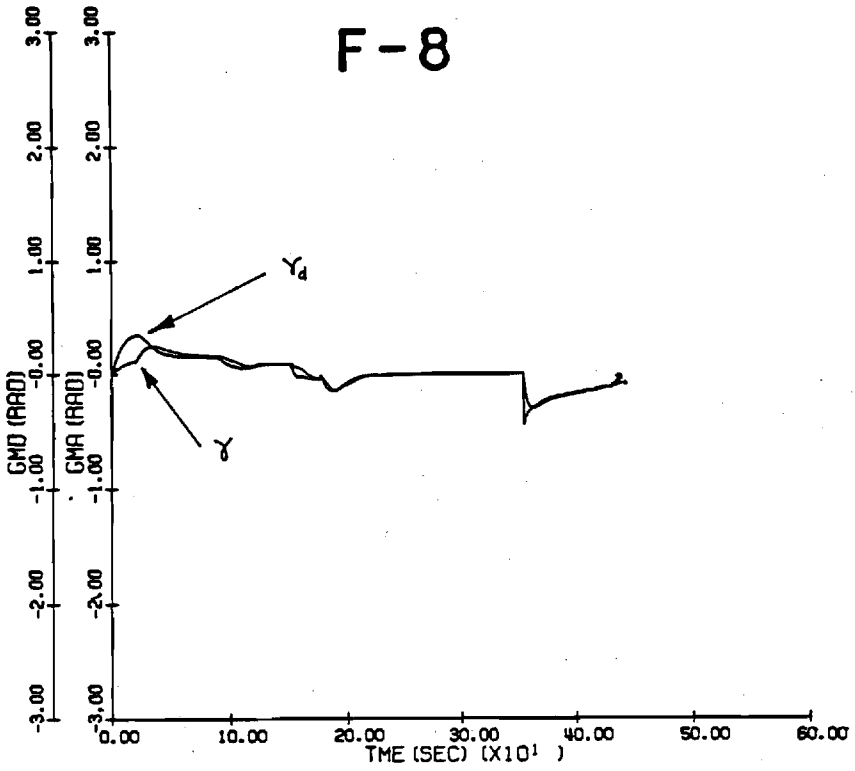

Figure 11. Desired and actual flight path angle profile for case 2

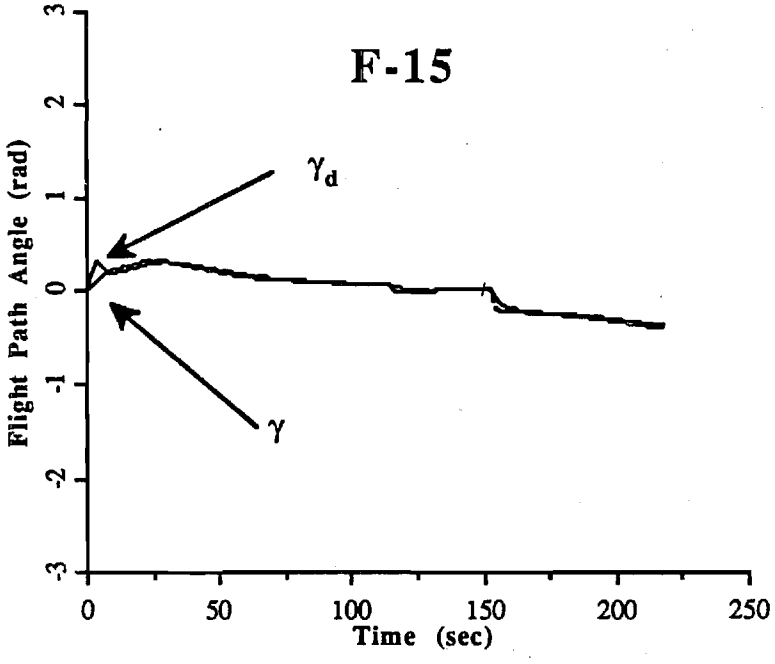

Figure 12. Desired and actual flight path angle profile for case 2

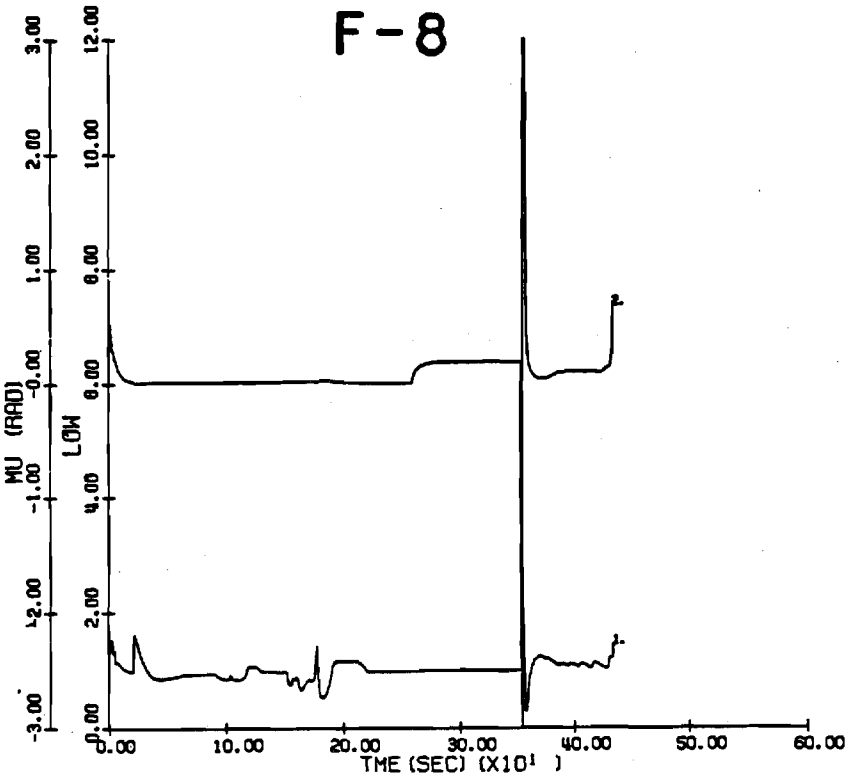

Figure 13. Lift and bank angle profile for case2

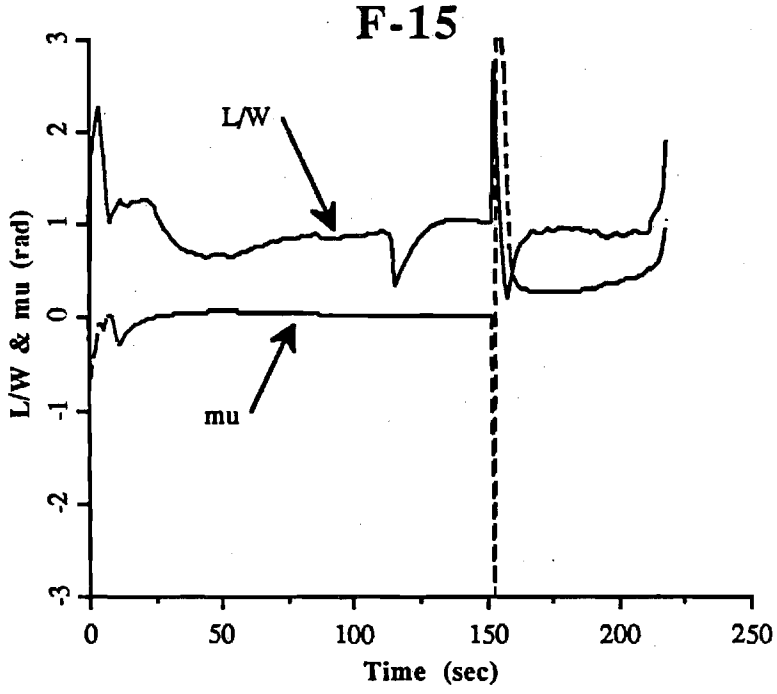

Figure 14. Lift and bank angle profile for case 2

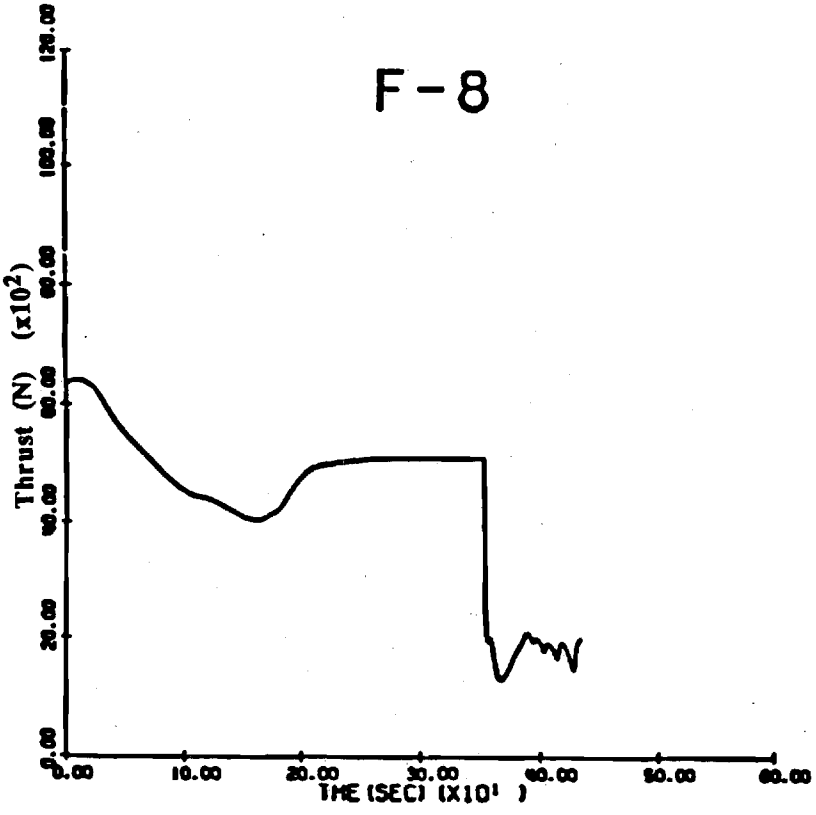

Figure 15. Thrust profile for case 2

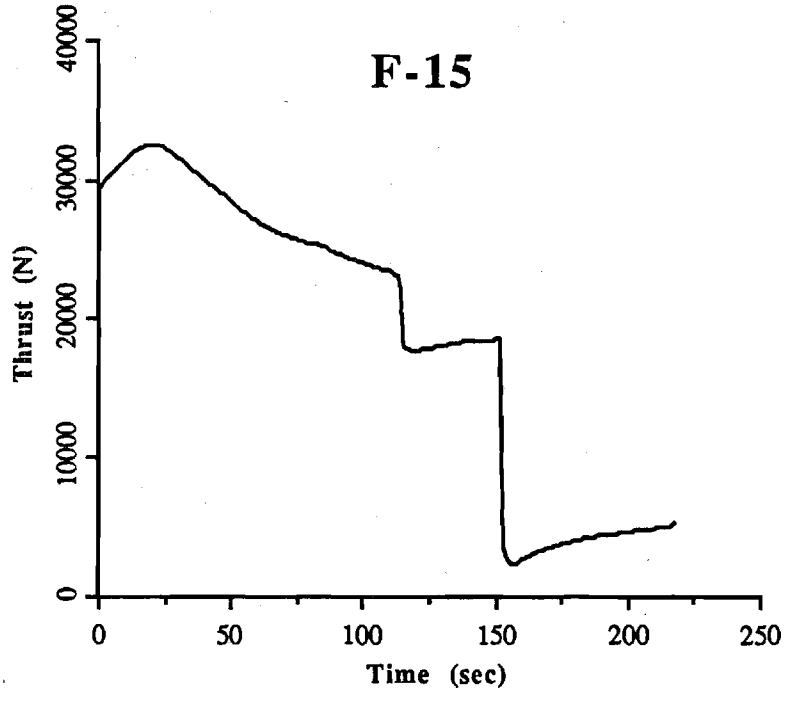

Figure 16. Thrust profile for case 2

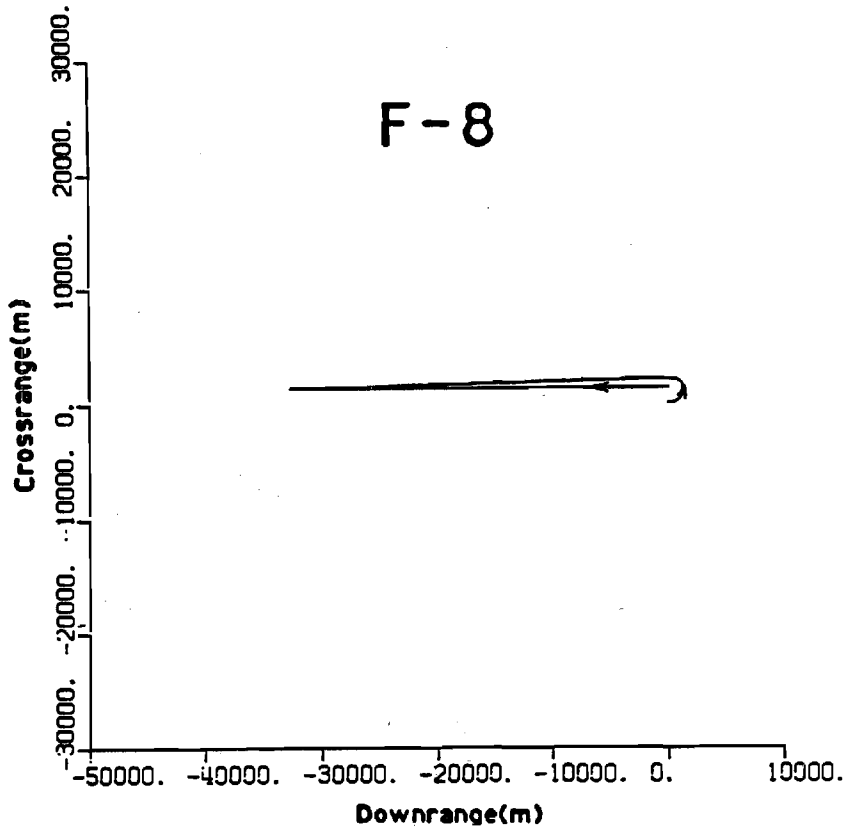

Figure 17. Ground track for case 4

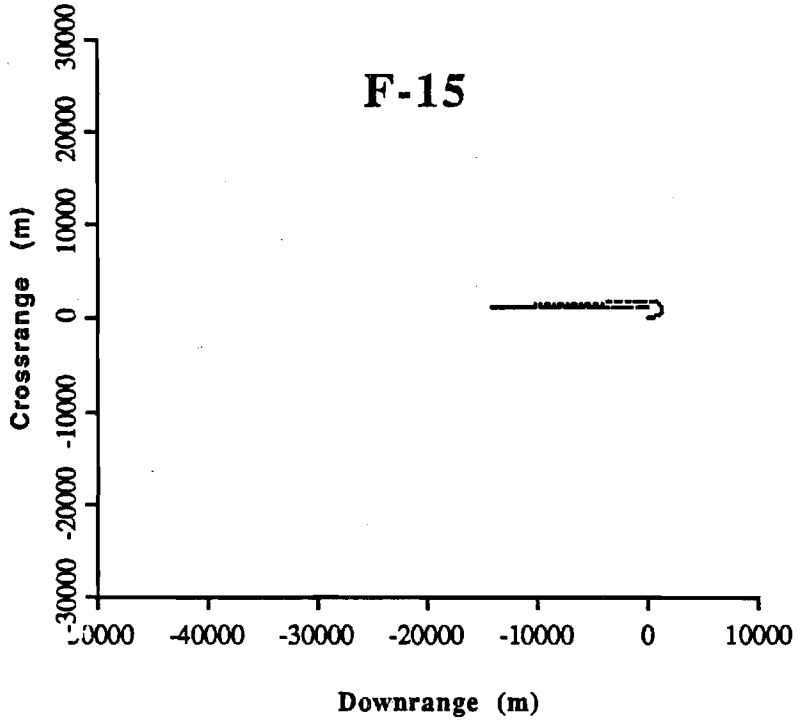

Figure 18. Ground track for case 4

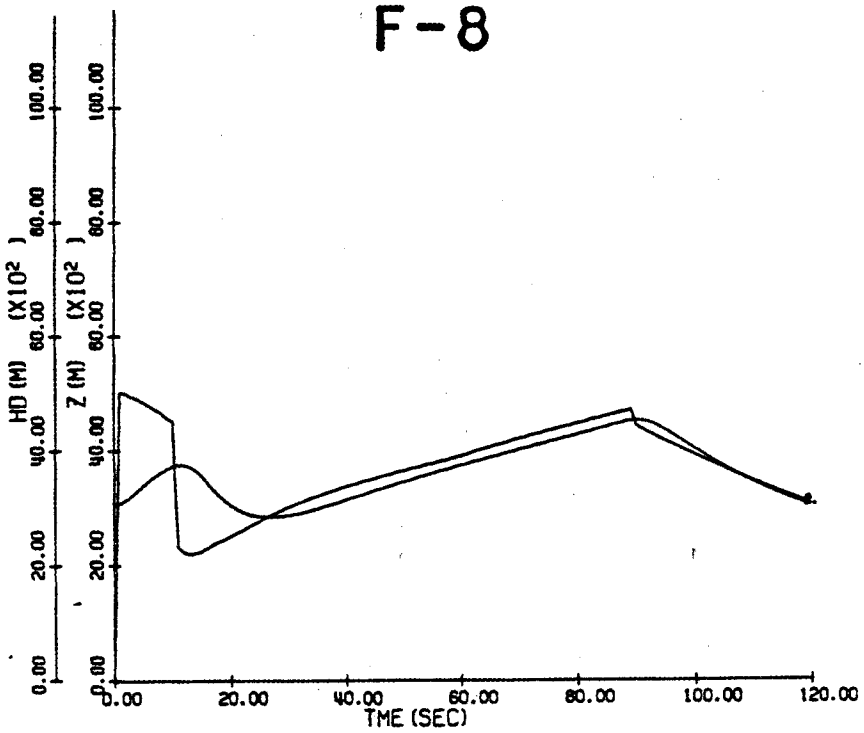

Figure 19. Commanded and actual altitude profiles for case 4

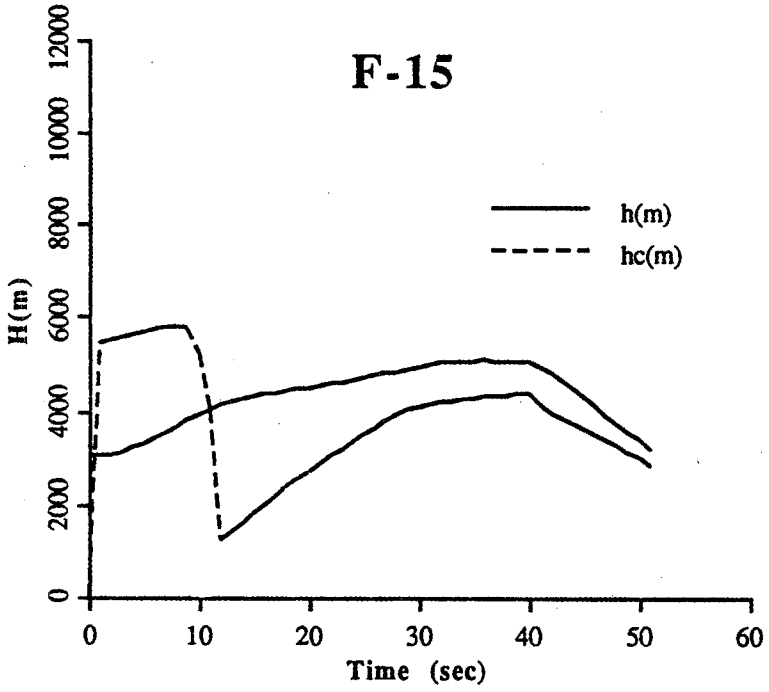

Figure 20. Commanded and actual altitude profiles for case 4

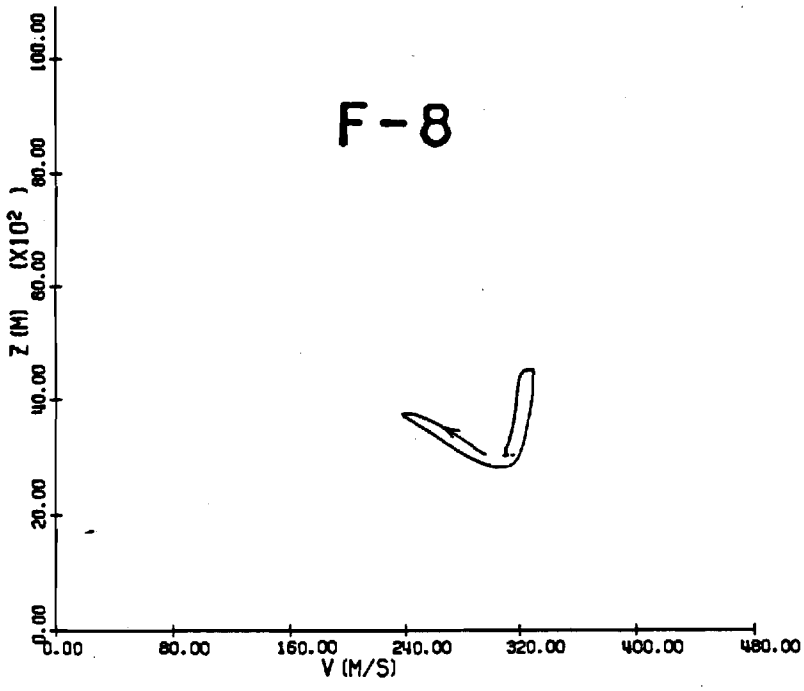

Figure 21. Altitude versus velocity for case 4

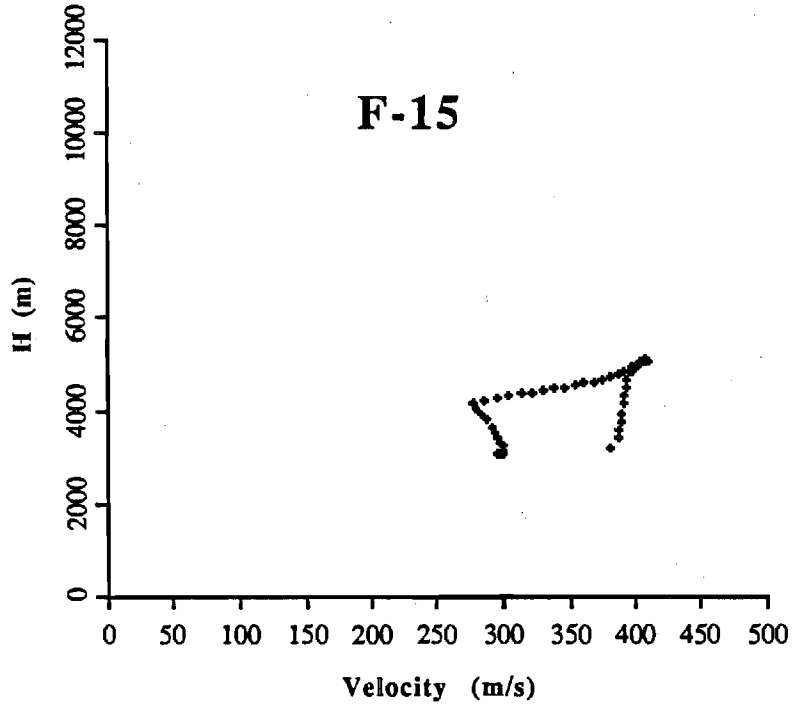

Figure 22 Altitude versus velocity for case 4

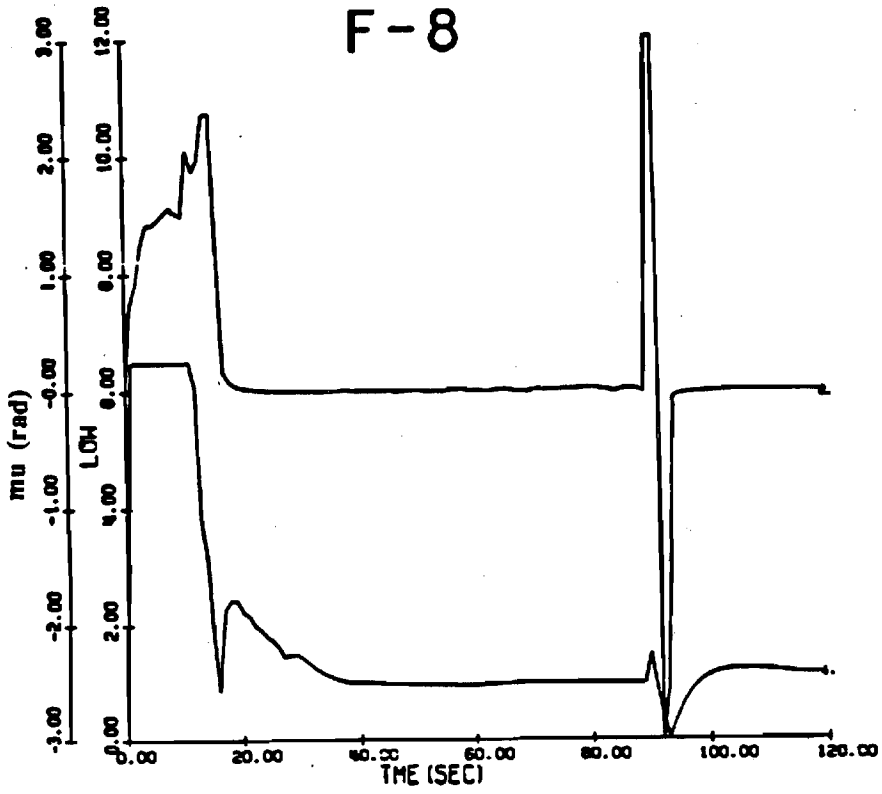

Figure 23. Lift and bank angle profile for case 4

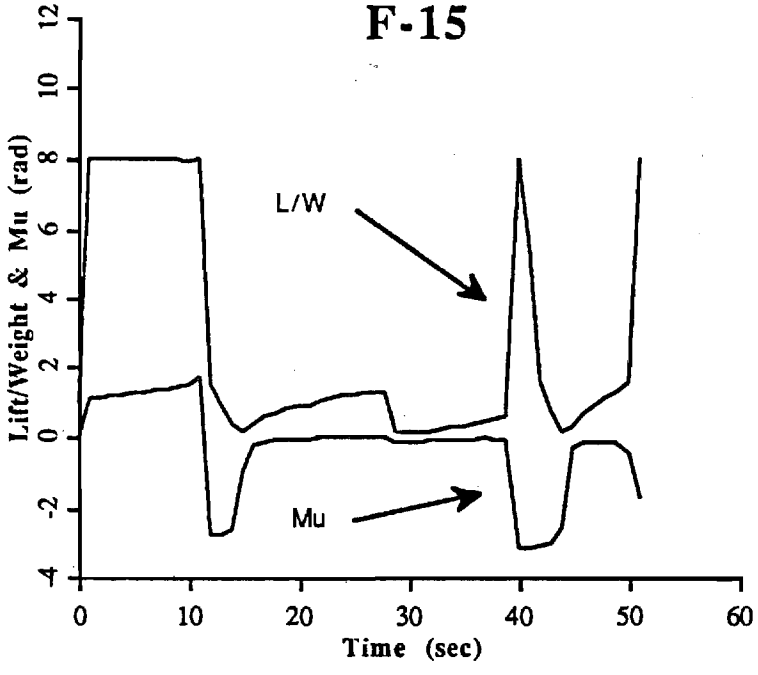

Figure 24. Lift and bank angle profile for case 4

Georgia Institute of Technology
A UNIT OF THE UNIVERSITY SYSTEM OF GEORGIA
ATLANTA, GEORGIA 30332

OFFICE OF CONTRACT ADMINISTRATION
Contracting Support Division

July 6, 1990

Phone: (404) 894-4764

REPLY TO: E-16-637

N.A.S.A.Ames-Dryden Flight Research Facility
Attn: Eugene L. Duke
Vehicle Technology Branch, D-OFV
Moffett Field, CA 94035

SUBJECT: Final Report-Part II
Project Directors:A.J.Calise and
P.K.A. Menon
Contract No.NCC 2-506
" Development of Aircraft Pursuit-
Evasion & Min-Time Interception
Algorithms "
period covered: 11/1/87-6/10/90

A Final Report was sent to you 2/9/90, written by A.J.Calise. At that time, we were unaware that P.K.A. Menon was in the process of writing a Part II. This should be the last report on this project.

The subject report is forwarded in conformance with the contract/grant specifications.

Should you have any questions or comments reguarding this report, please contact the Project Director or the undersigned.

Sincerely,

Mary M. Wolfe
Research Reports Coordinator

mmw
Distribution:
Addressee, 3 copies
NASA Sci.& Technical Inform.Ctr.-2 copies

Time-Optimal Aircraft Pursuit-Evasion with a Weapon Envelope Constraint - Final Report

June, 1990

Research Supported by
NASA Ames-Dryden Flight Research Facility
Grant No. NCC 2-506

Principal Investigator: P. K. A. Menon
NASA Grant Monitor: E. L. Duke

Georgia Institute of Technology
School of Aerospace Engineering
Atlanta, GA 30332

Time-Optimal Aircraft Pursuit-Evasion with A Weapon Envelope Constraint*

P. K. A. Menon
School of Aerospace Engineering
Georgia Institute of technology, Atlanta, GA 30332.
and
E. L. Duke
OFDC, NASA Ames-Dryden Flight Research Facility
Edwards, CA 93523

Abstract

Optimal pursuit-evasion problem between two aircraft including a realistic weapon envelope is analyzed using differential game theory. This study employs sixth order nonlinear point mass vehicle models and allows the inclusion of an arbitrary weapon envelope geometry. The performance index is a linear combination of flight time and the square of the vehicle acceleration. Closed form Solution to this high-order differential game is then obtained using feedback linearization. The solution is in the form of a feedback guidance law together with a quartic polynomial for time-to-go. Due to its modest computational requirements, this nonlinear guidance law useful for on-board real-time implementation.

Introduction

The objective of this paper is to develop an optimal nonlinear guidance scheme for aircraft pursuit-evasion using differential game theory [1] and the theory of feedback linearization [2,3]. This work extends previous research [4] to include time-of-flight in the performance index together with a realistic weapon envelope for the pursuing aircraft. Six state nonlinear point mass models of aircraft with lift, bank angle and throttle controls are employed in this work. The weapon envelope considered is an arbitrary three dimensional manifold with its origin at the vehicle center of gravity. This manifold may be specified as a function of the angle between the line-of-sight vector and the vehicle velocity vector, see Figure 1 for details. The *distance* between the two aircraft is then redefined as the difference between the relative position vector and components of the weapon effectiveness range measured from the pursuer's center of gravity. The pursuer attempts to drive this distance to zero while the evader attempts to make it as large as possible. The pursuit-evasion game terminates the first time instant this distance vector becomes zero. Both vehicles seek to accomplish their objectives in a time-optimal fashion while satisfying the limits on permissible acceleration levels. It is assumed in the present research that the evader has no offensive capabilities. As a result, this analysis includes only the pursuer's weapon envelope. Note that alternate approaches [5-8] may be required in the case where both vehicles have offensive capabilities. Additionally,

*Presented as a Paper at the 1990 American Control Conference, May 23 - 25, San Diego, CA

unlike Reference 5, it is assumed here that the weapon envelope cannot be oriented independent of the pursuer's velocity vector.

In the past, differential games of this nature could only be handled by linearizing the vehicle dynamics [9, 10] or by the use of simplified models [7, 12]. Differential game solutions obtained using linearized vehicle dynamics is of dubious value since it is not reasonable to define a nominal trajectory. Use of simplified vehicle models, on the other hand, can result in optimistic or pessimistic results depending on the region of validity of these models.

In practical applications, these factors have led to the formulation of such guidance problems as one-sided optimization problems, accurate only for dealing with nonmaneuvering targets. In order to handle actively maneuvering targets, it is necessary to formulate them as differential games. In this case, however, the numerical complexities preclude real-time implementation. Alternate approaches to these problems consist of off-line construction and storage of a field of extremals with real-time interpolation [12].

In Reference 4, it was shown that feedback solutions are feasible for a class of nonlinear differential games arising in aircraft pursuit-evasion. In that work, the performance index was required to be a quadratic form in the distance between two vehicles and the square of the magnitude of their acceleration. In [4], the nonlinear aircraft models were first transformed into a linear time-invariant form. A differential game was then formulated in transformed coordinates and solved. The resulting guidance law was transformed back to the original space to obtain the nonlinear pursuit-evasion guidance law. This research has been subsequently extended to study spacecraft pursuit-evasion and rendezvous problems [13, 14]. Solution to the differential game in this form requires the knowledge of time-to-go. In vehicle models without actuator saturation, this quantity can be computed exactly as outlined in Reference 13. Recently, the solution given in Reference 4 has been evaluated on a realistic simulation of high performance aircraft [15].

The objective of the present research is to extend this methodology to include time-of-flight in the performance index and a realistic weapon envelope in the model for the pursuing aircraft. Note that the results presented here may be adapted to one-sided guidance problems such as those discussed in References 16 and 17.

Nonlinear Models for the Pursuer and the Evader

The point-mass equations of motion for an aircraft are given by

$$\dot{V} = \frac{T(h, M, \eta) - D(h, M, L)}{m} - g \sin\gamma \tag{1}$$

$$\dot{\chi} = \frac{L \sin\phi}{mV \cos\gamma} \tag{2}$$

$$\dot{\gamma} = \frac{g}{V}\left(\frac{L \cos\phi}{W} - \cos\gamma\right) \tag{3}$$

$$\dot{x} = V \cos\gamma \cos\chi \tag{4}$$

$$\dot{y} = V \cos\gamma \sin\chi \tag{5}$$

$$\dot{h} = V \sin\gamma \tag{6}$$

The salient assumptions in this model are a flat non-rotating earth, thrust along the path and a quiescent atmosphere. In the equations (1)-(6), V is the airspeed, γ the flight path angle, χ heading angle, T the vehicle thrust, D vehicle drag, L the lift, g acceleration due to gravity, M the Mach number, and m is the vehicle mass. Position of the aircraft in an earth-fixed, inertial frame is given by the down-range x, cross-range y, and altitude h. The control variables in this model are the vehicle lift L, bank angle ϕ, and the throttle setting η. Note that the vehicle thrust is specified as a nonlinear function of altitude, Mach number and the throttle setting.

The aerodynamic drag is calculated using the drag coefficient C_D, the airspeed V, the atmosphere density ρ and the reference area s as

$$D = C_D s \rho V^2/2 \tag{7}$$

In (7), the drag coefficient C_D is a nonlinear function of the Mach number M and the lift L.

The equations of motion for the evader is in the same form as that of the pursuer. However, the thrust and drag characteristics may be different.

The Pursuer's Weapon Envelope

The present analysis will include a weapon envelope only for the pursuer. The evader is not assumed to have any offensive capabilities. A more complex formulation will be essential if one assumes the existence of offensive capabilities for the evader. In such a differential game, each participant may attempt to maximize the distance between itself and the other vehicle's weapon envelope, while attempting to drive the adversary into its own weapon envelope. Such a formulation may lead to the study of combat games or two-target games[5-8]. The present research will not address these issues. In all that follows, it will be assumed that the roles of each participant in the game is fixed and remains unchanged for the entire duration of the engagement.

As indicated in the foregoing, the evader is not assumed to have any offensive capabilities. As a result, if the pursuer is successful in bringing the evader within its weapon effectiveness range, then capture is said to have occurred. In the present research, pursuer's weapon envelope is assumed to be a three dimensional manifold with its origin located at the vehicle center of gravity. The weapon effectiveness range is defined as the distance between the vehicle center of gravity and the intersection of the three dimensional manifold defining the weapon envelope with the line-of-sight vector. Details are shown in Figure 1. The weapon effectiveness range is assumed to be a function of the angle between the vehicle velocity vector and the line-of-sight vector. Note that this modeling is consistent with the weapon usage envelope in currently operational fixed wing fighter aircraft.

It is assumed here that the weapon envelope cannot be oriented independent of the vehicle velocity vector. In flight vehicles such as combat helicopters and fighter aircraft with precision fuselage pointing capabilities, an alternate assumption might be more appropriate. Clearly, such capabilities provide additional degrees of freedom in controlling the outcome of the differential game.

In a chosen inertial frame, if the pursuer's velocity vector and the differential position vector between the pursuer and the evader are $[\dot{x}_p\ \dot{y}_p\ \dot{h}_p]^T$ and $[\Delta x\ \Delta y\ \Delta h]^T$ respectively, then the angle between the pursuer's velocity vector and the line-of-sight vector may be computed using the expression:

$$\cos\delta = \frac{\dot{x}_p\Delta x + \dot{y}_p\Delta y + \dot{h}_p\Delta h}{\sqrt{\Delta x^2 + \Delta y^2 + \Delta h^2}\sqrt{\dot{x}_p^2 + \dot{y}_p^2 + \dot{h}_p^2}} \tag{8}$$

In the expression (8), $\Delta h = h_e - h_p$, $\Delta x = x_e - x_p$, $\Delta y = y_e - y_p$. The angle δ is sometimes termed as the line-of-sight angle. The weapon effectiveness range R_w can then be specified as a function of the line-of-sight angle as :

$$R_w = F(\delta) \tag{9}$$

For example, if the weapon effectiveness envelope were a cone centered at the vehicle center of gravity, the weapon range may be described as follows:

$$R_w = r, \quad if \quad |\delta| \leq \delta_{max} \tag{10}$$

$$R_w = 0, \quad otherwise \tag{11}$$

The quantity r is a specified constant. A *prolate spheroid* with its major axis oriented along the vehicle velocity vector appears to be a more realistic weapon envelope shape. Note that in this case, the weapons will be effective to a certain degree in the tail aspect also. This is consistent with the existing tactical weapon effectiveness envelopes in operational fighter aircraft. Such a weapon envelope is illustrated in Figure 1. In this case, it is possible to write an explicit expression weapon effectiveness range as

$$R_w = \frac{A}{1 + B\cos\delta} \tag{12}$$

In this expression, A and B are two constants specifying the size and shape of the prolate spheroid. These constants may be related to the minimum and maximum weapon ranges R_{min}, R_{max} as:

$$A = \frac{2\ R_{min}\ R_{max}}{R_{min} + R_{max}} \tag{13}$$

$$B = \frac{R_{min} - R_{max}}{R_{min} + R_{max}} \tag{14}$$

Note that the present specification of the weapon envelope can include a kill probability distribution given as a function of the weapon range. Further, any alternate shape for the weapon effectiveness envelope can be included in the ensuing analysis. If the orientation of the line-of-sight vector in the given inertial frame is defined using two angles θ and μ such that

$$\theta = tan^{-1}\frac{\Delta h}{\sqrt{\Delta x^2 + \Delta y^2}} \tag{15}$$

$$\mu = tan^{-1}\frac{\Delta y}{\Delta x} \tag{16}$$

the components of the weapon effectiveness range can be resolved into three components in the earth fixed frame as

$$h_w = R_w \sin\theta \tag{17}$$

$$x_w = R_w \cos\theta \cos\mu \tag{18}$$

$$y_w = R_w \cos\theta \sin\mu \tag{19}$$

Next, these quantities may be used to redefine the three components of the relative position between the pursuer and evader as :

$$z_1 = x_p + \epsilon x_w - x_e \tag{20}$$

$$z_2 = y_p + \epsilon y_w - y_e \tag{21}$$

$$z_3 = h_p + \epsilon h_w - h_e \tag{22}$$

The variable ϵ multiplying the weapon envelope components is included in the foregoing to enable the adjustment of the relative weighting between the weapon envelope and the distance between the two vehicles. Such a trade-off is useful while considering the use of different weapon systems in a given pursuit-evasion scenario. From equations (20)-(22), it may be observed that the distance between the two vehicles can be altered either by changing the distance between the vehicle center of gravities or by orienting the weapon envelope. Both these quantities are directly influenced by the vehicle relative position, velocity, and acceleration components. Note that if the weapon envelope was independently orientable, then this relative distance will depend additionally on the orientation parameters. However, in all that follows, it will be assumed that the weapon envelope cannot be oriented independent of the vehicle velocity vector.

Next assume that the quantities x_w, y_w, h_w and their various time derivatives are available from on-board measurements. Examining the geometric relations (19)-(21), it may be observed that these quantities can be computed if the angles δ, θ, μ and their various time derivatives are available. The assumption that these quantities are available from measurements is crucial for including an arbitrary shaped weapon envelope in the derivation of the present guidance law. If these quantities are not available from on-board measurements, then only a spherical weapon envelope shape can be employed in the analysis. This is because of the fact that the second derivative of the line-of-sight angle depends on *jerk*. The presence of this term introduces difficulties in transforming the vehicle model into linear, time-invariant form as will be apparent in the next section.

An interesting extension of the formulation discussed in this section is the inclusion of a sensor effectiveness envelope in the analysis. In such a pursuit-evasion game, the maneuvers will not only be influenced by weapon envelope considerations, but also by information trade-offs. A familiar example of the control-information mini-maximization is the timed maximum lateral acceleration maneuver employed by fighter aircraft for missile evasion. The objective here is to take advantage of the fact that missile seeker tracking rate as well as the missile maneuvering capabilities are limited. Following the proposed methodology for the inclusion of the weapon envelope, it is possible to include a sensor effectiveness envelope in the present formulation. Additional situations where such constraints as these arise include the guidance of robots in the presence of workspace envelope and actuator constraints. These issues will not be pursued any further in the present paper.

Feedback linearization

The chief difficulty in obtaining solutions to differential games using realistic flight vehicle models is that these models are highly nonlinear. Moreover, classical linearization approach using Taylor series expansion is invalid in a differential game setting [7], primarily due to the difficulty in defining a *nominal* trajectory. However, it can be shown[4] that if the differential game between the two vehicles is formulated in terms of the position state variables and their various derivatives, then feedback linearization approach can be used to obtain a nonlinear feedback solution. The primary thrust of the present research is to extend the work in Reference 4 to include the time-of-flight in the performance index and a weapon envelope in the vehicle model. Feedback linearization is then used to transform the vehicle dynamic models into a linear, time-invariant form. The pursuit-evasion game is formulated in terms of

the transformed states and solved to obtain the guidance law. Inverse transformation of this guidance law to the original coordinates produces an implementable nonlinear guidance scheme.

As in Reference 4, feedback linearization is accomplished by differentiating the equations (20)-(22) twice with respect to time and substituting for $\dot{V}, \dot{\gamma}, \dot{\chi}$ from expressions (1)-(3). interpreting the right hand sides of the resulting expressions as the new control variables in the problem, one has :

$$\dot{z}_1 = Z_1, \quad \dot{Z}_1 = U_1 + \epsilon V_1 - W_1 \tag{23}$$

$$\dot{z}_2 = Z_2, \quad \dot{Z}_2 = U_2 + \epsilon V_2 - W_2 \tag{24}$$

$$\dot{z}_3 = Z_3, \quad \dot{Z}_3 = U_3 + \epsilon V_3 - W_3 \tag{25}$$

where

$$U_1 = \frac{(T_p - D_p)}{m_p} \cos\gamma_p \cos\chi_p - \frac{L_p}{m_p}(\sin\gamma_p \cos\chi_p \cos\phi_p + \sin\chi_p \sin\phi_p) \tag{26}$$

$$U_2 = \frac{(T_p - D_p)}{m_p} \cos\gamma_p \sin\chi_p + \frac{L_p}{m_p}(\cos\chi_p \sin\phi_p - \sin\gamma_p \sin\chi_p \cos\phi_p) \tag{27}$$

$$U_3 = \frac{(T_p - D_p)}{m_p} \sin\gamma_p + \frac{L_p}{m_p} \cos\gamma_p \cos\phi_p - g \tag{28}$$

$$V_1 = \ddot{x}_w, \; V_2 = \ddot{y}_w, \; V_3 = \ddot{h}_w \tag{29}$$

$$W_1 = \frac{(T_e - D_e)}{m_e} \cos\gamma_e \cos\chi_e - \frac{L_e}{m_e}(\sin\gamma_e \cos\chi_e \cos\phi_e + \sin\chi_e \sin\phi_e) \tag{30}$$

$$W_2 = \frac{(T_e - D_e)}{m_e} \cos\gamma_e \sin\chi_e + \frac{L_e}{m_e}(\cos\chi_e \sin\phi_e - \sin\gamma_e \sin\chi_e \cos\phi_e) \tag{31}$$

$$W_3 = \frac{(T_e - D_e)}{m_e} \sin\gamma_e + \frac{L_e}{m_e} \cos\gamma_e \cos\phi_e - g \tag{32}$$

Note that the new control variables $U_i, W_i, i = 1, 2, 3$ depend on the system states and the original control variables. If the parameter ϵ is set to zero, the model (23)-(25) will turn out to be identical to that given in Reference 4. It is assumed here that the various derivatives of the weapon envelope components x_w, y_w, h_w are available from on-board measurements. In the general case, these derivatives will depend on the vehicle position, velocity, acceleration, jerk and various time derivatives of jerk. As a result, if these quantities are not available as measurements, the feedback linearization implied by the expressions (23)-(25) will not be feasible. In that case, the ensuing analysis will permit only the use of a spherical weapon envelope.

With the interpretation of $U_1 + \epsilon V_1, U_2 + \epsilon V_2, U_3 + \epsilon V_3, W_1, W_2, W_3$ as the new control variables, the equations (23)-(25) describe a linear time-invariant system. Given the pseudo-control variables, the real control variables in the system can be computed using the relations [4]:

$$\phi_p = tan^{-1}\left[\frac{U_2 \cos\chi_p - U_1 \sin\chi_p}{\cos\gamma_p(U_3 + g) - \sin\gamma_p(U_1 \cos\chi_p + U_2 \sin\chi_p)}\right] \tag{33}$$

$$L_p = \frac{m_p[\cos\gamma_p(U_3+g) - \sin\gamma_e(U_1\cos\chi_p + U_2\sin\chi_p)]}{\cos\phi_p} \tag{34}$$

$$T_p = \Big[\sin\gamma_p(U_3+g) + \cos\gamma_p(U_1\cos\chi_p + U_2\sin\chi_p)\Big]m_p + D_p \tag{35}$$

The corresponding expressions for the evader's control variables can be obtained by replacing U_1, U_2, U_3 by W_1, W_2, W_3 and changing the state variable subscripts as follows :

$$\phi_e = tan^{-1}\left[\frac{W_2\cos\chi_e - W_1\sin\chi_e}{\cos\gamma_e(W_3+g) - \sin\gamma_e(W_1\cos\chi_e + W_2\sin\chi_e)}\right] \tag{36}$$

$$L_e = \frac{m_e[\cos\gamma_e(W_3+g) - \sin\gamma_e(W_1\cos\chi_e + W_2\sin\chi_e)]}{\cos\phi_e} \tag{37}$$

$$T_e = \Big[\sin\gamma_e(W_3+g) + \cos\gamma_e(W_1\cos\chi_e + W_2\sin\chi_e)\Big]m_e + D_e \tag{38}$$

Physically, the pseudo-control variables U_i, W_i, $i = 1,2,3$ are the acceleration components of the vehicle in the chosen inertial frame. Since the magnitude of a vector is invariant under coordinate transformation, the magnitudes of U, W are also the pursuer-evader acceleration magnitudes in the flight path axis system.

The attitude dynamics of the pursuer and the evader were not included in the foregoing analysis. Note that these may be included at the expense of increased model complexity. The primary reason for including these in a differential game would be to study the various information trade-offs involved in a typical pursuit-evasion scenario. For instance, if the pursuer's weapons employed an active radar seeker, then its maneuvers would be influenced by the fact that the maximum target area must be visible at all times. The evader, on the other hand, would employ an opposite strategy. Several interesting variations of this differential game can be studied in the present setting.

Guidance Law for Aircraft Pursuit-Evasion

The previous section dealt with an approach for making the nonlinear aircraft models amenable to analysis. In this section, the pursuit-evasion differential game will be formulated in the transformed coordinates and solved. Inverse transformation of this solution to the original coordinates yields the nonlinear feedback guidance law. In the following development it will be assumed that all the state variables required for computing the feedback law are known perfectly. Once the differential game is solved with perfect information, the effects of incomplete or imperfect information can be investigated using this solution.

The first issue in differential games is that of role definition. There is a controversy on this issue currently. But if the roles are assigned at the outset, the resulting differential game is amenable to analysis via Isaac's theory [1]. Assuming that the roles have been defined, the objective of the pursuer is to minimize the specified performance index which the evader tries to maximize. The performance index employed in the present research is:

$$\min_{(U+\epsilon V)}\max_{W}\int_0^{t_f}\Big\{\zeta + \frac{(1-\zeta)}{2}\Big[a[(U_1+\epsilon V_1)^2 + (U_2+\epsilon V_2)^2 + (U_3+\epsilon V_3)^2] - b[W_1{}^2 + W_2{}^2 + W_3{}^2]\Big]\Big\}dt \tag{39}$$

The final time t_f is unspecified. This performance index is to be optimized by the two participants subject to the differential constraints (23)-(25). In (39), ζ defines the relative weighting between flight time and acceleration magnitude, while the positive quantities a and b serve to constrain the acceleration magnitudes of the pursuer and the evader. For reasons that will be made clear in the ensuing, it is assumed that

$$b > a, \quad 0 < \zeta < 1 \tag{40}$$

The negative sign in front of the evader's acceleration term explicitly identifies this player as the maximizer. Initial values on all the state variables are assumed known. The pursuit-evasion maneuvers are terminated the first time instant the evader makes contact with the pursuer's weapon envelope, viz.

$$z_{1f},\ z_{2f},\ z_{3f} = 0 \tag{41}$$

where

$$z_{1f} = z_1(t_f),\ z_{2f} = z_2(t_f),\ z_{3f} = z_3(t_f)$$

The final value of the relative velocities Z_1, Z_2, Z_3 are assumed to be free. Next, define the variational Hamiltonian as:

$$H = \zeta + \frac{1}{2}(1-\zeta)\Big\{a[(U_1+\epsilon V_1)^2 + (U_2+\epsilon V_1)^2 + (U_3+\epsilon V_1)^2] - b[{W_1}^2 + {W_2}^2 + {W_3}^2]\Big\}$$

$$+\lambda_1 Z_1 + \lambda_2 Z_2 + \lambda_3 Z_3 + \lambda_4(U_1+\epsilon V_1 - W_1) + \lambda_5(U_2+\epsilon V_2 - W_2) + \lambda_6(U_3+\epsilon V_3 - W_3) \tag{42}$$

As in Reference 4, the objective of the present research is obtain a saddle-point solution to the differential game. The conditions under which such a solution may exist are well known [18]. The central requirement here is the separability of the variational Hamiltonian with respect to the pursuer and the evader state and control variables. In the present case, inspection of the variational Hamiltonian defined in (38) will reveal that such a separability exists. The saddle point solution can be found by proceeding formally as follows.

The costate equations [10] for this problem can be obtained as

$$\dot{\lambda}_1 = \dot{\lambda}_2 = \dot{\lambda}_3 = 0 \tag{43}$$

$$\dot{\lambda}_4 = -\lambda_1,\ \dot{\lambda}_5 = -\lambda_2,\ \dot{\lambda}_6 = -\lambda_3 \tag{44}$$

The optimality conditions yield :

$$U_1 + \epsilon V_1 = \frac{-\lambda_4}{a(1-\zeta)} \tag{45}$$

$$U_2 + \epsilon V_2 = \frac{-\lambda_5}{a(1-\zeta)} \tag{46}$$

$$U_3 + \epsilon V_3 = \frac{-\lambda_6}{a(1-\zeta)} \tag{47}$$

$$W_1 = \frac{-\lambda_4}{b(1-\zeta)} \tag{48}$$

$$W_2 = \frac{-\lambda_5}{b(1-\zeta)} \tag{49}$$

$$W_3 = \frac{-\lambda_6}{b(1-\zeta)} \tag{50}$$

Since the final values of Z_1, Z_2, Z_3 are free, the costates $\lambda_4, \lambda_5, \lambda_6$ are zero at the final time. This fact, together with equations (45)-(50) imply that the pseudo control variables are all zero at the final time. Integrating the costate equations (44) and using the boundary conditions on $\lambda_4, \lambda_5, \lambda_6$ yields

$$\lambda_4 = \lambda_1(t_f - t) \tag{51}$$

$$\lambda_5 = \lambda_2(t_f - t) \tag{52}$$

$$\lambda_6 = \lambda_3(t_f - t) \tag{53}$$

Using the expressions (51) - (53) to eliminate the costates on the right hand side of the optimality conditions (45) - (50) one has :

$$\dot{Z}_1 = \frac{\lambda_1}{(1-\zeta)}[\frac{1}{b} - \frac{1}{a}](t_f - t) \tag{54}$$

$$\dot{Z}_2 = \frac{\lambda_2}{(1-\zeta)}[\frac{1}{b} - \frac{1}{a}](t_f - t) \tag{55}$$

$$\dot{Z}_3 = \frac{\lambda_3}{(1-\zeta)}[\frac{1}{b} - \frac{1}{a}](t_f - t) \tag{56}$$

Expressions (54)-(56) may next be integrated to obtain Z_1, Z_2, Z_3. Due to the symmetry of the solution to this problem, only one component of the solution will be fully illustrated in the ensuing. Thus :

$$Z_1 = Z_1(0) + \frac{\lambda_1}{(1-\zeta)}[\frac{1}{b} - \frac{1}{a}](t_f t - \frac{t^2}{2}) \tag{57}$$

Integrating the expression (57) yields

$$z_1(t) = z_1(0) + Z_1(0)t + \frac{\lambda_1}{(1-\zeta)}[\frac{1}{b} - \frac{1}{a}](t_f \frac{t^2}{2} - \frac{t^3}{6}) \tag{58}$$

Using the game termination condition (41) in the expression (58) yields

$$\lambda_1 = -\frac{3(1-\zeta)ab}{(a-b){t_f}^3}\Big[z_1(0) + Z_1(0)t_f\Big] \tag{59}$$

This may next be substituted in the optimality conditions to obtain the optimal control for the pursuer as

$$U_1 + \epsilon V_1 = \frac{3b}{(a-b){t_f}^3}\Big[z_1(0) + Z_1(0)t_f\Big](t_f - t) \tag{60}$$

The optimal control for the evader is given by

$$W_1 = \frac{3a}{(a-b){t_f}^3}\Big[z_1(0) + Z_1(0)t_f\Big](t_f - t) \tag{61}$$

The remaining control variables in the problem can be similarly computed. The solution is incomplete at this stage since the final time t_f is unknown. This quantity may be computed by invoking a constant of motion in this problem. Since the final time is open and the variational Hamiltonian is autonomous, one has that

$$H(t) = 0 \tag{62}$$

Substituting for the optimal controls in terms of costates in the constant of motion (62) at the initial time results in

$$\begin{aligned} 0 = \zeta + \frac{1}{2(1-\zeta)}[\frac{1}{b} - \frac{1}{a}]\Big\{{\lambda_4}^2 + {\lambda_5}^2 + {\lambda_6}^2\Big\} \\ +\lambda_1 Z_1(0) + \lambda_2 Z_2(0) + \lambda_3 Z_3(0) \end{aligned} \tag{63}$$

Next, substituting for $\lambda_4, \lambda_5, \lambda_6$ from expressions (51) - (53) yields

$$\begin{aligned} 0 = \zeta + \frac{1}{2(1-\zeta)}[\frac{1}{b} - \frac{1}{a}]\Big\{{\lambda_1}^2 + {\lambda_2}^2 + {\lambda_3}^2\Big\}{t_f}^2 \\ +\lambda_1 Z_1(0) + \lambda_2 Z_2(0) + \lambda_3 Z_3(0) \end{aligned} \tag{64}$$

Finally, substituting for $\lambda_1, \lambda_2, \lambda_3$ in terms of initial states from expression (59) yields a quartic polynomial of the form

$${t_f}^4 + q_2{t_f}^2 + q_1 t_f + q_0 = 0 \tag{65}$$

where

$$q_2 = [Z_1(0)^2 + Z_2(0)^2 + Z_3(0)^2]/\frac{2\zeta}{3(1-\zeta)}\Big[\frac{1}{b} - \frac{1}{a}\Big] \tag{66}$$

$$q_1 = 4[Z_1(0)z_1(0) + Z_2(0)z_2(0) + Z_3(0)z_3(0)]/\frac{2\zeta}{3(1-\zeta)}\Big[\frac{1}{b} - \frac{1}{a}\Big] \tag{67}$$

$$q_0 = 3[z_1(0)^2 + z_2(0)^2 + z_3(0)^2]/\frac{2\zeta}{3(1-\zeta)}\Big[\frac{1}{b} - \frac{1}{a}\Big] \tag{68}$$

The smallest positive value of the final time emerging from the polynomial (65) should be used in subsequent calculations. Note that the parameter ζ should satisfy the in equality (40) to ensure that these polynomial coefficients remain finite. Additionally, the polynomial coefficients q_0 and q_2 will be negative if $b > a$. Since the coefficient corresponding to ${t_f}^3$ is zero and the coefficients q_0, q_2 are negative, the Hurwitz criterion [19] in the theory of polynomials implies that this polynomial has roots with positive real parts. Next, forming the Routh array [19], the first column turns out to be

$$[1,\ \kappa,\ -q_1/\kappa,\ q_1,\ q_0]^T \tag{69}$$

Here, κ is a small positive parameter and the superscript T denotes the transpose. If q_1 is less than zero, this array suggests that one root of the polynomial (65) will have a positive real part. On the other

hand, if $q_1 > 0$, three roots of this polynomial will have positive real parts. Since complex roots always occur in conjugate pairs, the foregoing observations imply that the polynomial (65) will produce at least one usable value of t_f. Note that the final time t_f has to be iteratively determined. However, since the objective is to determine the smallest positive real root of this polynomial, a one dimensional search scheme is adequate.

An interesting special case occurs if q_1 were zero. Note that the numerator of the coefficient q_1 is simply the inner product of relative position and velocity vectors at the initial time. If these two vectors are orthogonal, the coefficient q_1 will be zero. This condition can be seen to be satisfied in various commonly encountered engagement scenarios, one of them being the case of pursuer and evader being instantaneously located at the same down-range-cross-range positions while in level flight at different altitudes and airspeeds. In these cases, the quartic (65) can be solved for in closed form. All the roots of (65) may be computed using the expression

$$t_{go}{}^2 = \frac{-q_2 \pm \sqrt{q_2{}^2 - 4q_0}}{2} \tag{70}$$

Both q_2 and q_0 will be negative if $b > a$. In this case, the right hand side of (70) will be strictly real.

Finally, in order to convert the control laws (56), (57) to explicit feedback form, assume that that the current time t is the initial time. In this case, the quantities $(t_f - t)$, t_f may both be replaced by time-to-go t_{go}. Additionally, as discussed elsewhere in this paper, the weapon envelope components V_1, V_2, V_3 are assumed to be available from measurements. Using these, one has

$$U_1 = \frac{3b}{(a-b)t_{go}{}^2}\left[z_1 + Z_1 t_{go}\right] - \epsilon V_1 \tag{71}$$

$$U_2 = \frac{3b}{(a-b)t_{go}{}^2}\left[z_2 + Z_2 t_{go}\right] - \epsilon V_2 \tag{72}$$

$$U_3 = \frac{3b}{(a-b)t_{go}{}^2}\left[z_3 + Z_3 t_{go}\right] - \epsilon V_3 \tag{73}$$

$$W_1 = \frac{3a}{(a-b)t_{go}{}^2}\left[z_1 + Z_1 t_{go}\right] \tag{74}$$

$$W_2 = \frac{3a}{(a-b)t_{go}{}^2}\left[z_2 + Z_2 t_{go}\right] \tag{75}$$

$$W_3 = \frac{3a}{(a-b)t_{go}{}^2}\left[z_3 + Z_3 t_{go}\right] \tag{76}$$

This completes the solution of the differential game in the feedback linearized coordinates. However, this solution is usable only after transformation to the original coordinates. This transformation may be achieved by substituting the expressions (71)-(76) in the expressions (33)-(38) given in the previous section. However, in order to conserve space, this step will not be carried out here.

The guidance laws resulting from the foregoing algebraic manipulations are highly nonlinear and coupled. They use full state feedback along with vehicle performance related quantities such as thrust, drag, and mass for generating the minimax optimal feedback control settings for the pursuer and the evader. It is not difficult to show that these solutions satisfy the Strengthened Legendre-Clebsch necessary condition if $a > 0$, $b > 0$. Investigation of additional second-order necessary conditions and a detailed examination of the saddle point properties of this solution will be of future interest.

Numerical Evaluation

The nonlinear guidance law developed in this paper was implemented on a point-mass simulation of two aircraft. The vehicle data used for both aircraft is similar that of a high performance aircraft used in previous aircraft pursuit-evasion studies [4,15]. The equations of motion were integrated using a fourth-order Runge-Kutta method and the aerodynamic coefficients and the thrust limits were linearly interpolated from a stored table. The time-to-go quartic (65) was solved using the Newton's method with zero as the initial guess. The derivatives of the weapon envelope components required in the guidance law computations were obtained using a second-order linear observer of the form

$$\ddot{x}_{wo} = \omega^2(x_w - x_{wo}) - 2\nu\omega\dot{x}_{wo} \tag{77}$$

$$\ddot{y}_{wo} = \omega^2(y_w - y_{wo}) - 2\nu\omega\dot{y}_{wo} \tag{78}$$

$$\ddot{h}_{wo} = \omega^2(h_w - h_{wo}) - 2\nu\omega\dot{h}_{wo} \tag{79}$$

In (77)-(79), ω, ν are the observer natural frequency and the damping ratio, respectively. The values used in the present numerical study are $\omega = 10, \nu = 1$. This observer uses the weapon envelope components x_w, y_w, h_w as the inputs to form the derivative estimates $\dot{x}_{wo}, \dot{y}_{wo}, \dot{h}_{wo}, \ddot{x}_{wo}, \ddot{y}_{wo}, \ddot{h}_{wo}$. These estimates are then used in computing the controls for the pursuer and the evader.

Although several runs have been made, results from one engagement scenario will only be presented in the ensuing. In this study, a highly eccentric prolate spheroid weapon envelope with its major axis aligned along the pursuer's velocity vector was considered. This weapon envelope had a minimum range of 10 m and a maximum range of 500 m. The two vehicles are initially separated by 2000 m in down range and 5000 m in cross range, with the pursuer behind the evader. The pursuer's velocity vector is initially aligned along the down range direction, while the evader's velocity vector points along the cross range direction at the initial time. The pursuer has an initial velocity is 160 m/s while flying level at 16 km altitude. The evader has an initial velocity of 110 m/s at an altitude of 10 km, with zero flight path angle. The present study employed a weighting factor of $a = 0.01$ for the pursuer and $b = 0.03$ for the evader. The weight on the flight time was $\zeta = 0.5$. The engagement time corresponding to these initial conditions and the given weights computed from the quartic (65) turns out to be 50.79 seconds. The weapon envelope weighting factor $\epsilon = 1$ was used in this analysis.

Figure 2 illustrates the trajectories of both the pursuer and the evader in the cross-range down-range plot. Triangular markers are provided every 5 seconds to give an idea about the relative position of the two vehicles. To further aid in interpreting these trajectories, the flight time is indicated at 10 second intervals along the pursuer-evader trajectories. The turn-dash behavior of both the pursuer and the evader noted in previous studies [4, 12, 15] is apparent from this figure. The altitude histories corresponding to this engagement are given in Figure 3. Both the pursuer and the evader have negative flight path angles at the time of capture. The heading angle histories for both vehicles are given in Figure 4. From this figure, it is clear that the pursuer is attempting to continuously avoid a heading angle match. The airspeed histories for the two vehicles given in Figure 5 shows the pursuer slowing down during the initial portion of the turn followed by an acceleration. The evader, on the other hand, is accelerating through most of the engagement. The load factor, throttle setting and the bank angle for both the pursuer and the evader are shown in Figures 6, 7, 8. From these figures, it may be observed that both the pursuer and the evader are executing a descending turn. In order to illustrate the influence of the weapon envelope on the engagement, a plot of the acceleration history along the altitude direction is given in Figure 9. If the weapon envelope were spherical, the acceleration history would have been a straight line, as is the case

for the evader. However, the presence of the prolate spheroid envelope introduces strong nonlinearities in the acceleration history. The performance of the pursuit-evasion guidance law is apparent from these plots. Evaluation of these guidance laws in a more complex vehicle simulation is currently under way.

Conclusions

This paper presented the development of feedback guidance laws for aircraft pursuit-evasion. The analysis employed nonlinear point-mass models of aircraft. A realistic weapon effectiveness envelope was included in the analysis. Assuming that the weapon envelope components may be computed from given measurements, the vehicle model was transformed to a linear, time invariant form. The pursuit-evasion differential game was formulated using this model and the solution obtained. The performance index employed consisted of a linear combination of flight time and the square of the vehicle acceleration. Inverse transformation of this solution produces a nonlinear guidance law together with a quartic for the computation of the free final time. This guidance law is in closed-loop state feedback form and uses the vehicle performance data. Modifications of the present guidance law to include a sensor effectiveness envelope were sketched.

Numerical results using high performance aircraft data were given. Since the computational requirements for the guidance law are modest, it appears that this solution is implementable on-board aircraft.

References

[1] Isaacs, R., *Differential Games*, Robert E. Krieger, Huntington, New York, 1965.

[2] Brockett, R. W., "Nonlinear Systems and Differential Geometry", *Proceedings of the IEEE*, Vol. 64, Feb. 1976, pp. 61-72.

[3] Hunt, L. R., Su, R., and Meyer, G., "Global Transformations of Nonlinear Systems", *IEEE Transactions on Automatic Control*, Vol. , Jan. 1983, pp. 24-31.

[4] Menon, P. K. A., "Short-Range Nonlinear Feedback Strategies for Aircraft Pursuit-Evasion", *Journal of Guidance, Control and Dynamics*, Jan.-Feb. 1989, pp. 27-32.

[5] Heymann, M., Ardema, M. D., and Rajan, N., "A Formulation and Analysis of Combat Games", NASA TM 85927, April 1984.

[6] Getz, W. M., and Pachter, M., "Capturability in a Two-Target Game of Two Cars", *Journal of Guidance and Control*, Vol. 4, Jan.- Feb. 1981, pp.15-21.

[7] Davidovitz, A., and Shinar, J., "Eccentric Two-Target Model for Qualitative Air Combat Game Analysis", *Journal of Guidance, Control, and Dynamics*, Vol. 8, May-June 1985, pp. 325-331.

[8] Ghose, G., and Prasad, U. R.,"Analysis of Security Strategies for a two Target Game", *AIAA Guidance, Navigation and Control Conference*, Aug. 14-16, 1989, Boston, MA, paper 89-3597.

[9] Anderson, G. M., "Comparison of Air-to-Air Missile Guidance Laws based on Optimal Control and Differential Game Theory", *Proceedings of the AIAA Guidance, and Control Conference*, August 1979, Paper No. 79-1736.

[10] Bryson, A. E., and Ho, Y. C., *Applied Optimal Control*, Hemisphere, Washington, 1975.

[11] Kelley, H. J., and Lefton, L., "Estimation of Weapon-Radius Vs Maneuverability Tradeoff for Air-to-Air Combat", *AIAA Journal*, Vol. 15, Feb. 1977, pp. 145-148.

[12] Ardema, M. D., Rajan, N., and Yang, L., "Three-Dimensional Energy-State Extremals in Feedback Form", *Journal of Guidance, Control and Dynamics*, July-Aug. 1989, pp. 601-605.

[13] Menon, P. K. A., and Calise, A. J., "Interception, Evasion, Rendezvous, and Velocity-to-be-Gained Guidance for Spacecraft", *AIAA Guidance, Navigation, and Control Conference*, Monterey, CA., Aug. 1987.

[14] Menon, P. K. A., Calise, A. J., and Leung, S. K. M., "Guidance Laws for Spacecraft Pursuit-Evasion and Rendezvous", *AIAA Guidance, Navigation, and Control Conference*, Minneapolis, MN, Aug. 1988.

[15] Williams, P. S., Antoniewicz, R. F., Duke, E. L., and Menon, P. K. A.,"Study of a Pursuit-Evasion Guidance law for High Performance Aircraft", *1989 American Control Conference*, Pittsburgh, PA, June 21-23, 1989.

[16] Calise, A. J., "Singular perturbation Techniques for On-line Optimal Flight Path Control", *Journal of Guidance and Control*, Vol. 4, July-Aug. 1981, pp. 398-405.

[17] Menon, P. K. A., and Briggs, M. M., "Near-Optimal Midcourse Guidance for Air-to-Air Missiles", to appear in the *Journal of Guidance, Control and Dynamics.*

[18] Friedmann, A., *Differential Games*, Academic Press, New York, 1971.

[19] Kuo, B. C., *Automatic Control Systems*, Prentice-Hall, New York, 1967.

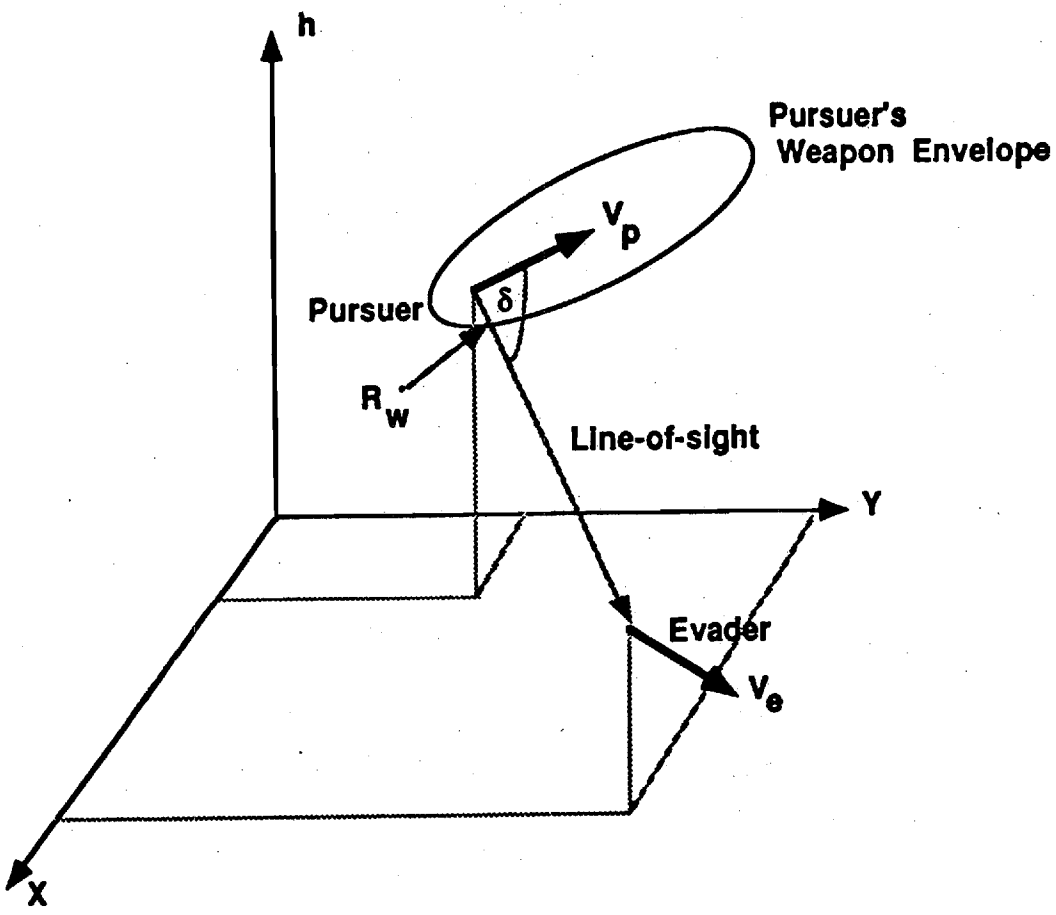

Fig. 1. The Coordinate System

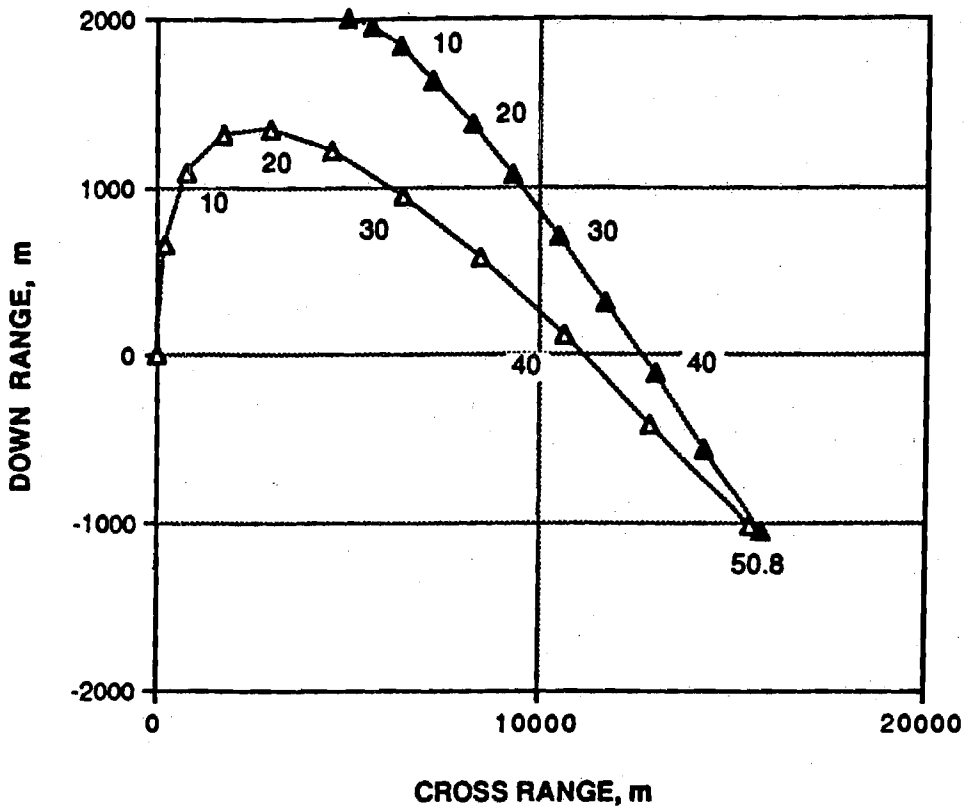

Fig. 2. Pursuer-Evader Trajectories in the Horizontal Plane. Dark Triangle : Evader, Light Triangle : Pursuer.

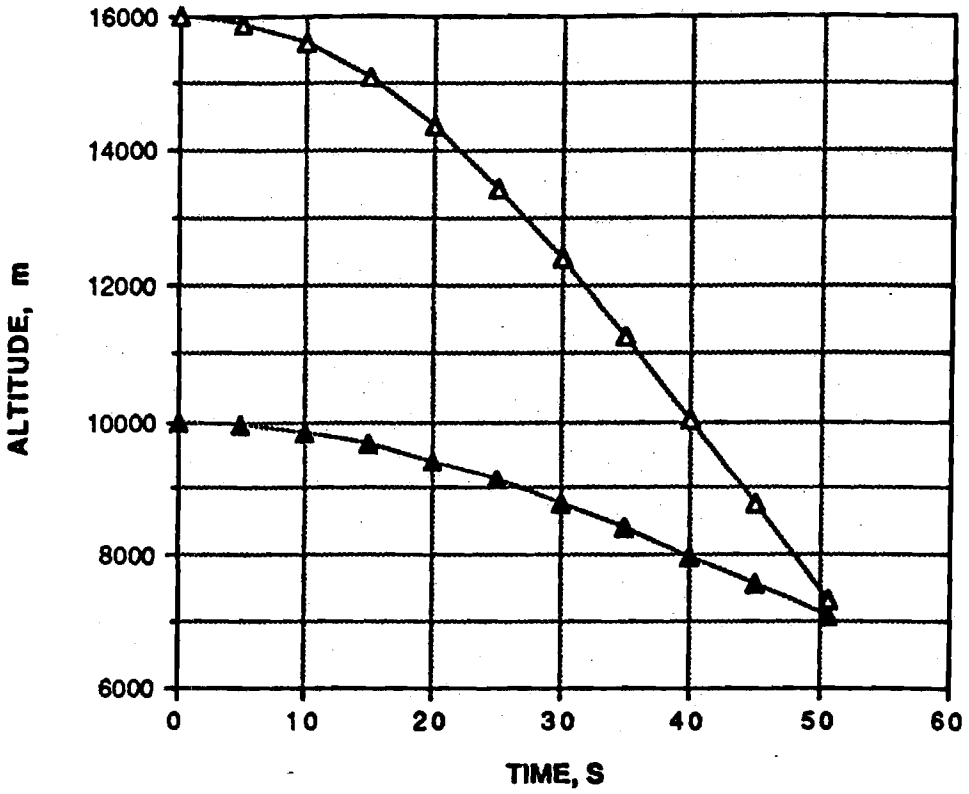

Fig. 3. Temporal Evolution of Pursuer-Evader Altitudes. Dark Triangle : Evader, Light Triangle : Pursuer.

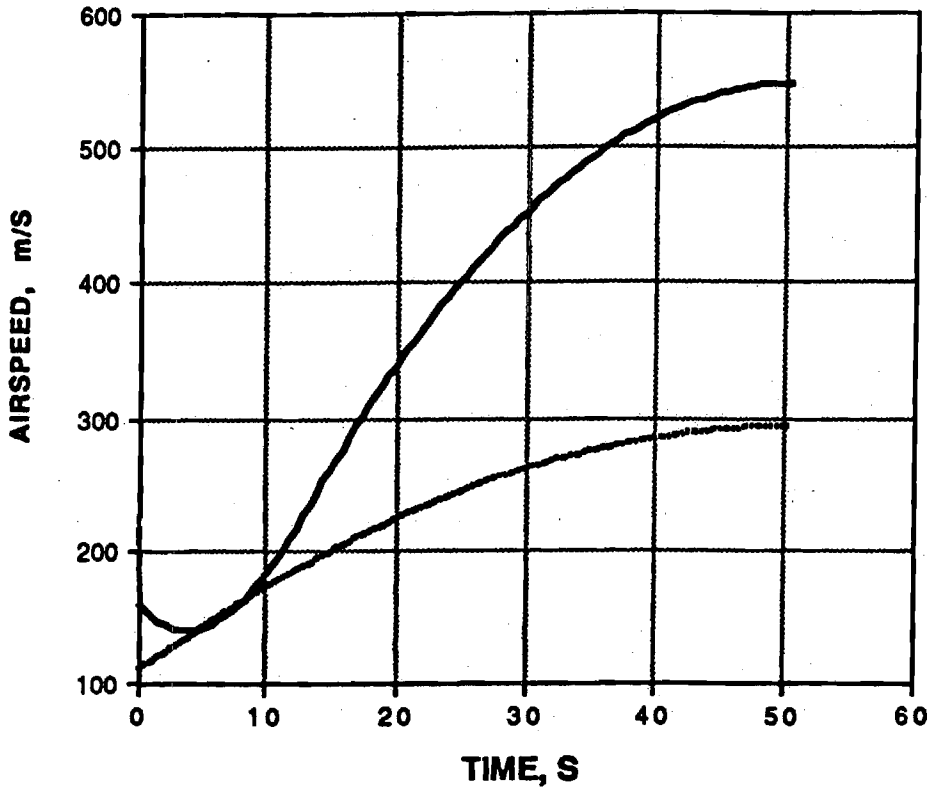

Fig. 4. Temporal Evolution of Pursuer-Evader Airspeeds. Dotted Line : Evader, Solid Line : Pursuer.

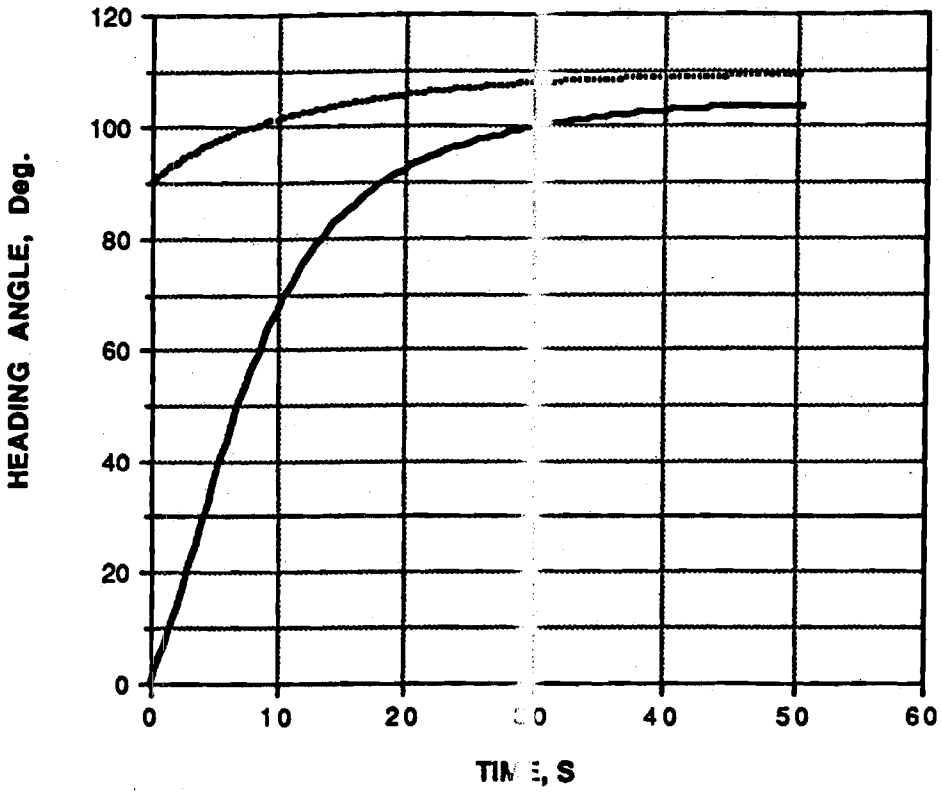

Fig. 5. Heading Angle Historie: for the Pursuer and the Evader. Dotted Line : Evader, S lid Line : Pursuer.

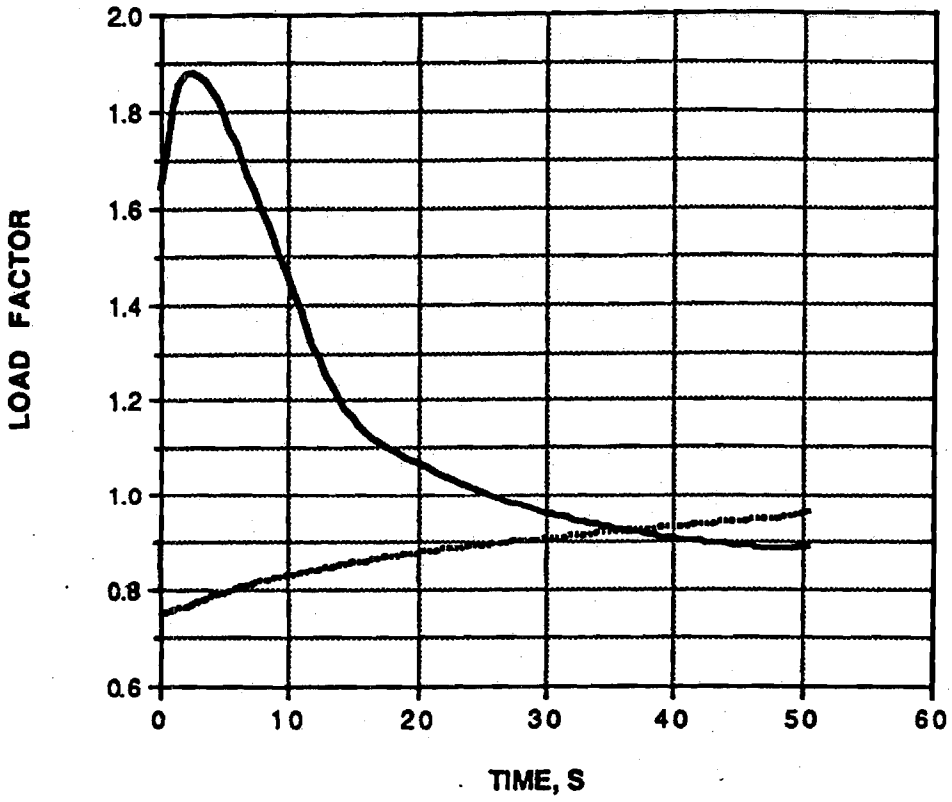

Fig. 6. Load Factor Histories for the Pursuer and the Evader.
Dotted Line : Evader, Solid Line : Pursuer.

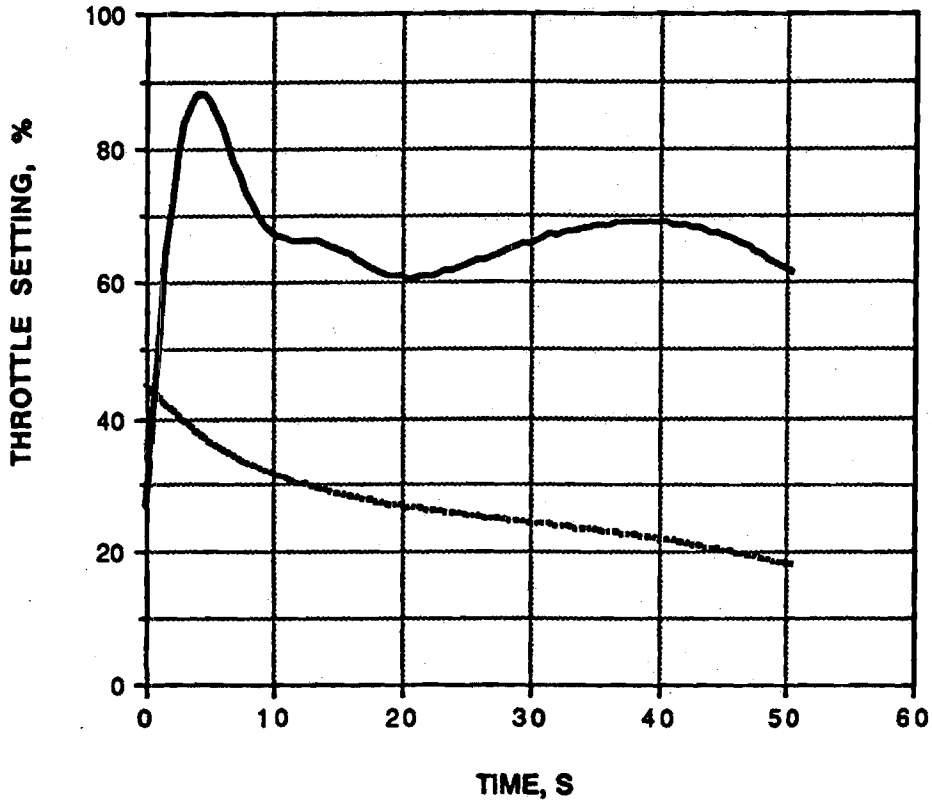

Fig. 7. Temporal Evolution of Pursuer-Evader Throttle Setting. Dotted Line : Evader, Solid Line : Pursuer.

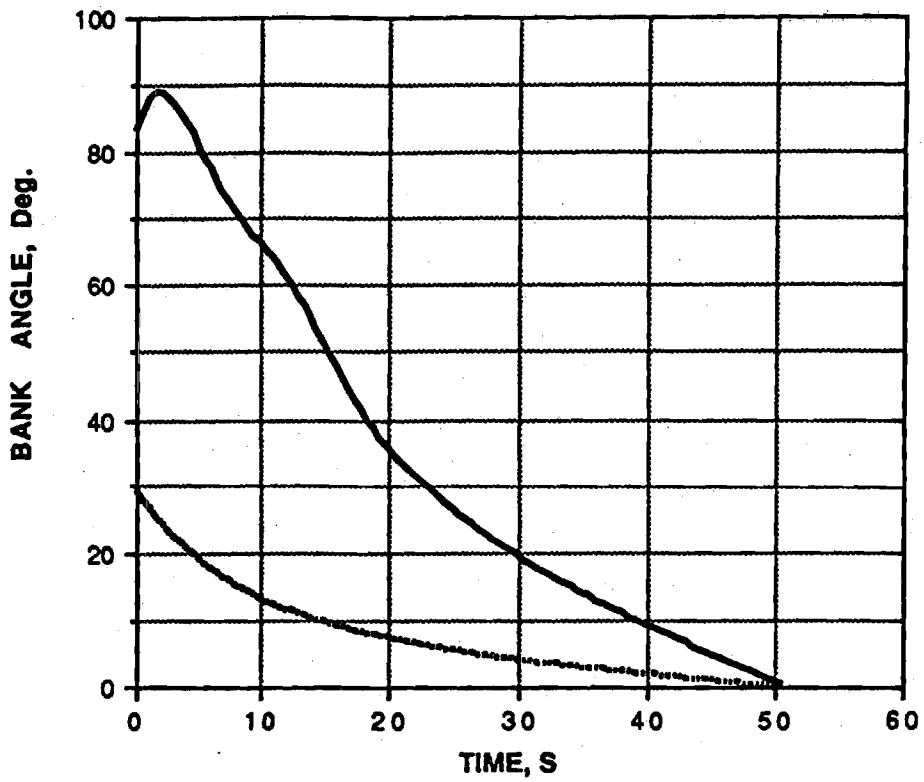

Fig. 8. Bank Angle Histories for the Pursuer and the Evader.
Dotted Line : Evader, Solid Line : Pursuer.

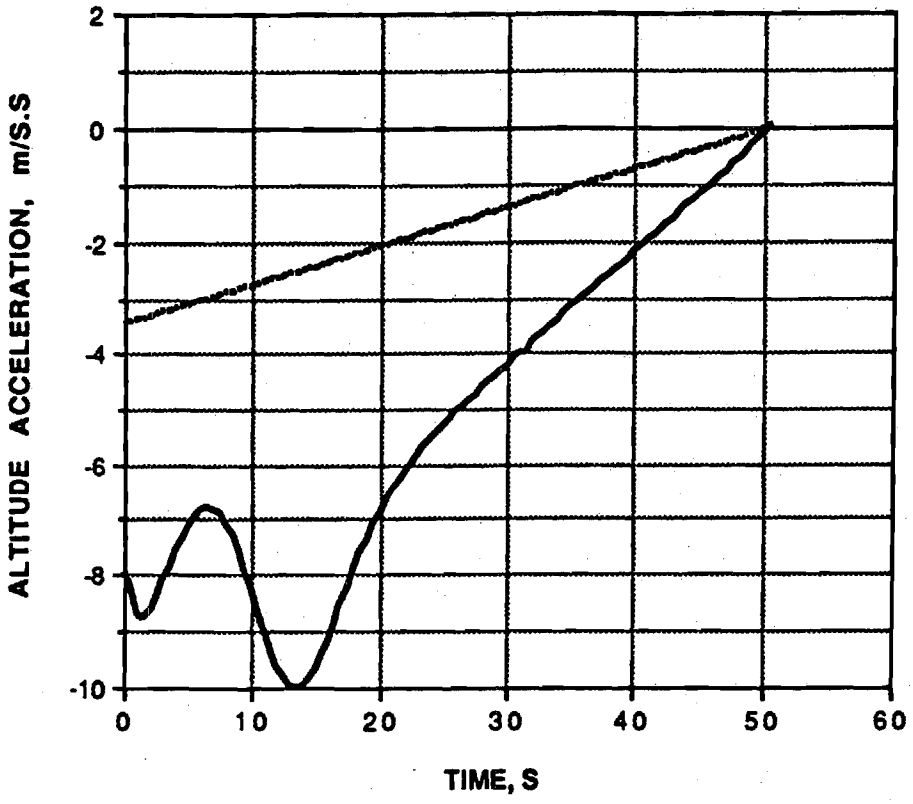

Fig. 9. Altitude Acceleration Histories for the Pursuer and the Evader. Dotted Line : Evader, Solid Line : Pursuer.